

2012

# Microstructure and mechanical properties of cold drawn steel wires

Ning Liu  
*Edith Cowan University*

---

## Recommended Citation

Liu, N. (2012). *Microstructure and mechanical properties of cold drawn steel wires*. Retrieved from <https://ro.ecu.edu.au/theses/512>

This Thesis is posted at Research Online.  
<https://ro.ecu.edu.au/theses/512>

# Edith Cowan University

## Copyright Warning

You may print or download ONE copy of this document for the purpose of your own research or study.

The University does not authorize you to copy, communicate or otherwise make available electronically to any other person any copyright material contained on this site.

You are reminded of the following:

- Copyright owners are entitled to take legal action against persons who infringe their copyright.
- A reproduction of material that is protected by copyright may be a copyright infringement. Where the reproduction of such material is done without attribution of authorship, with false attribution of authorship or the authorship is treated in a derogatory manner, this may be a breach of the author's moral rights contained in Part IX of the Copyright Act 1968 (Cth).
- Courts have the power to impose a wide range of civil and criminal sanctions for infringement of copyright, infringement of moral rights and other offences under the Copyright Act 1968 (Cth). Higher penalties may apply, and higher damages may be awarded, for offences and infringements involving the conversion of material into digital or electronic form.

EDITH COWAN UNIVERSITY  
FACULTY OF COMPUTING, HEALTH AND SCIENCE  
SCHOOL OF ENGINEERING

# **Microstructure and Mechanical Properties of Cold Drawn Steel Wires**

NING LIU

Student No.:10205055

Supervisor: A/Professor Laichang Zhang

Associate-supervisor: Dr Zonghan Xie (The University of Adelaide)

This thesis is presented in fulfilment of the requirements for the  
Degree of Master of Engineering Science

Aug 2012

## USE OF THESIS

The Use of Thesis statement is not included in this version of the thesis.

## Abstract

Cold drawn eutectoid steel wires have been widely used for a variety of applications, such as suspension bridges, steel cords for automobile tires, and springs. Much research has been done to increase their mechanical strength. With advances in modern production technology, both the drawing speed and the quality of drawn steels have been enhanced.

After a careful literature survey, it is obvious that some issues are still controversial. As Y.S. Yang, J.G. Bae and C.G. Park mentioned, the lamellar spacing, thickness and volume fraction of cementites have all reached the nanometer regime, and the conventional theory is not enough to explain it. Besides, the cementite dissolution is a huge problem to the performance, according to Y.S. Yang and C.G. Park.

To address the above issues, a systematic study has been taken on the wire drawing process under the conditions of the industrial production. Through the morphology, microscopic, mechanical and comprehensive analysis, a clear understanding of the microstructures and associated processing conditions of the high-strength carbon steel wires has been obtained.

This project aims to clarify why the mechanical properties improve with the increasing strain. The project will be carried out in four stages: 1) characterisation of the microstructure of the cold drawn steel wires; 2) measurements of the modulus, hardness and toughness of steel wires; 3) modelling the deformation behaviour of the cold drawn steels.

The techniques involved in the project include X-ray diffraction (XRD), focus ion beam (FIB), scan electron spectrum (SEM), Nanoindentation.

A deep understanding of the relationship between composition, structure and performance will be achieved in this project. The results may provide the basis for improving cold-drawn steel wire designs.

**Key words:** *drawn steel, pearlite, mechanical property, residual stress, deformation behaviour*

## ACKNOWLEDGEMENTS

Firstly, I would like to express my deepest thanks to Associate professor Laichang Zhang, my supervisor, for his close and enthusiastic support during the course of this project. Besides academic skills, he helps me build a new outlook on many things in life. A supervisor who is not only deals with the project problems, but tries to be helpful in other aspects and I really appreciate the beauty of his mannerism.

I would like to give my gratitude to my co-supervisor, Dr Zonghan Xie, for his kind supervision. His conscientious attitude towards research opens the door of research for me, though the beginning of the journey was not easy. I have learnt a lot, and am very grateful for the opportunities I have been given.

Thanks Dr Jerry Luo who is working in Curtin University. It has been my honour to work with him especially the parts of FIB and SEM in this project.

Many people from different professional contributed in different but meaningful ways to my thesis, especially Dr Xiaoli Zhao. A special word of appreciation goes to the IT staff, Mr. Kouroshe Sheikhzadeh and Zhihuan Yu for their unrelenting support at all times and stages in the development of my thesis.

I also wish to acknowledge the dedication of the administrative staff, especially Muriel Vaughan and Kim Gardiner. All these people have tremendous impact on my work. Indeed they understood the needs of a research student and were always available to meet them.

Finally, I wish to thank the many people I have had the pleasure of meeting during my work. Without the help and the friendship of these people, this thesis would never be completed. I, as well as, anyone who gains from reading the words herein owe them a debt of gratitude.

Ning Liu

## **Declaration**

I certify that this thesis does not, to the best my knowledge and belief:

I Incorporated without acknowledgement any material previously submitted for a degree or diploma in any institution of higher education.

II. Contain any material previously published or written by author person except where due reference is made in the text.

III. Contain any defamatory material.

I also grant permission for the Library at the Edith Cowan University to make duplicate copies of my thesis as required.

Signature:

Date:

# LIST OF FIGURES

Fig 2.1 the SEM pictures from the longitudinal (A, C, E, G) and transverse sections (B, D, F, H) of the drawn steel wires in different strain: $\epsilon=0$ (A, B), $\epsilon=0.7$ (C, D), $\epsilon=1.5$ (E, F) and $\epsilon=2.7$ (G, H).....	4
Fig 2.2 TEM micrographs and diffraction patterns obtained from the pearlitic steel wire.....	5
Fig 2.3 Schematic diagram of pearlitic morphology change.....	7
Fig 2.4 Analysis of cold drawing pearlitic steel.....	8
Fig. 2.5 Ne field ion micrographs of the pearlitic steel wires.....	9
Fig 2.6 segregation of carbon atoms on planar defects as labelled 1, 2 and 3.....	10
Fig 2.7 HRTEM micrograph of amorphous region in cold drawn wire ( $\epsilon = 3.6$ ).....	10
Fig 2.8 Free energy vs. composition for the ferrite-cementite system.....	13
Fig 2.09 Relationship between carbon concentration and the occurrence of delimitation.....	14
Fig 2.10 Effect of total strain on ultimate tensile strength of pearlite steel wires.....	16
Fig 3.1 The schematic of the drawing process.....	20
Fig 3.2 Geometry of XRD.....	21
Fig 3.3 Interference of X-ray on atomic multilayer.....	22
Fig 3.4 Schematic of the lift-out FIB technique for a film on a substrate.....	24
Fig 3.5 TEM specimen prepared by FIB milling.....	25
Fig 3.6 A schematic representation of the experimental apparatus used to perform the indentation experiments: (A) sample; (B) indenter; (C) load application coil; (D) indentation column guide springs; (E) capacitive displacement sensor.....	26
Fig 3.7 Typical load-displacement curve.....	27
Fig 4.1 the microstructure of the original wire.....	29
Fig 4.2 microstructure of wire after drawing.....	30
Fig 4.3 Microstructure of wire after drawing.....	30
Fig 4.4 Microstructure of wire.....	31
FIG 4.5 the morphology of pearlite after deformation (cross section).....	32
Fig 4.6 the morphology of pearlite before deformation (long section).....	32
Fig4.7 the lamellar spacing.....	34
Fig 5.1 Schematic illustration of the unloading process showing parameters characterizing the contact geometry.....	36
Fig 5.2 the pictures of the hardness in steel wires.....	38

Fig 5.3 the pictures of modulus in steel wires.....	40
Fig 5.4 XRD plot of $\alpha$ -Fe {110} before and as-deformed in long section.....	41
Fig5.5 XRD plot of $\alpha$ -Fe {200} before and as-deformed in long section.....	42
Fig 5.6 XRD plot of $\alpha$ -Fe {211} before and as-deformed in long section.....	42
Fig 5.7 XRD plot of $\alpha$ -Fe before and as-deformed in cross section.....	43
Fig 6.1 the SEM pictures after FIB cutting from the original steel wires.....	45
Fig 6.2 the SEM pictures after FIB cutting from the Middle-deformed steel wires.....	46
Fig 6.3 the SEM pictures after FIB cutting from the deformed steel wires.....	47
FIG7.1 Schematic illustration of contact between a spherical indenter and a flat specimen.....	50
FIG7.2 the SEM pictures for the loading intents.....	50
FIG7.3 the stress-strain curve from nanoindentation after the deformation.....	51
Fig 7.4 the stress-strain curve from nanoindentation before the deformation.....	52
Fig 7.5 the model for the steel wires as a composite material.....	53

# TABLE OF CONTENTS

## Contents

USE OF THESES .....	I
Abstract.....	II
ACKNOWLEDGEMENTS.....	III
Declaration.....	IV
LIST OF FIGURES .....	V
TABLE OF CONTENTS.....	VII
CHAPTER 1 Introduction.....	1
1.1 General .....	1
1.2 Research questions.....	1
1.3 Objectives and Scope of the Present Work .....	2
CHAPTER 2 Literature Review .....	3
2.1 The microstructure of the drawn steel.....	3
2.2 The Picture from SEM .....	3
2.3 The lamellar deformation characteristics in drawn steel wires .....	5
2.4 The study on the cementite dissolution in the cold drawn pearlitic steel wire .....	7
2.5 The mechanism of the dissolution of the cementite.....	11
2.5.1 Dislocation binding mechanism .....	11
2.5.2 The mechanism of interfacial energy .....	13
2.6 The change of the mechanical properties of steel wires.....	14
2.7 The strengthening mechanisms of the cold-drawing pearlitic steel wires .....	15
2.8 The research content and significance .....	17
CHAPTER 3 Approach and Methodology .....	20

3.1 General .....	20
3.2 The research methodology .....	21
3.2.1 the metallograph.....	22
3.2.2 X-ray diffraction (XRD) .....	22
3.2.3 Focused Ion Beam (FIB).....	24
3.2.4 Nanoindentation test.....	26
CHAPTER 4 The Microstructure of Drawn Steel Wires.....	29
4.1 General .....	29
4.2 The metallographic analysis.....	30
4.3 SEM observations .....	31
4.4 Lamellar spacing changes .....	33
CHAPTER 5 The Mechanical Prosperities of Steel Wires.....	37
5.1 Hardness and Modulus from nanoindentation .....	37
5.1.1 General .....	37
5.1.2 Hardness .....	38
5.1.3 Modulus.....	40
5.2 XRD .....	42
5.3 Conclusion.....	44
CHAPTER 6 Microstructure from FIB.....	45
6.1 General .....	45
6.2 FIB Pictures.....	45
CHAPTER 7 The Stress-Strain Curve From Nanoindentation and The Modelling for The Steel Wires .....	50
7.1 The stress-strain curve.....	50
7.2 The modelling for the steel wires .....	53

CHAPTER 8 Summary and Conclusion.....	56
8.1 summary.....	56
8.2 conclusions.....	56
8.3 Recommendation for Future Work .....	57
CHAPTER 9 References.....	58

# CHAPTER 1 Introduction

## 1.1 General

The combination of good ductility in torsion and excellent mechanical properties makes the drawn steel wires have become one of the best engineering materials for many industrial applications. The study on high-carbon steel can be traced to 1960s with the understanding the details of microstructural evolution during cold drawing of pearlitic steel wires [1-5]. In recent years, a great number of researchers have concentrated on the importance of understanding the evolution of the cementite phase during the deformation [6-9]. Considerable work has been performed to increase the tensile strength of high-carbon steel wires; the record of maximum experimental value is 5.7 GPa [10]. In order to increase the properties suitable for various working environments, one research direction on the drawn steel wires is to figure out the microstructure and the texture evolution in the process of cold deformation of drawn steel wire [8]. Owing to the deformation of cementite occurred in drawn process, this topic have drawn considerable attraction both in science and technology.

However, limited experimental work has been conducted to investigation of the microstructure and the texture evolution in the process of cold deformation of drawn steel wire. In addition, more work on processing and predicting good products is needed. The present work aimed to investigate the mechanical properties of drawn steel wires in varying drawing strains by nanoindentation tests as well as by microstructural observations. Our modeling showed the arrangement of ferrite and cementite in steel wires with different strains.

## 1.2 Research questions

The following issues will be investigated in the project:

What is the composition of the drawn steel in the five different kinds of samples?

What is the difference in the microstructure of the five different kinds of samples?

Mechanical properties such as pearlite size, preferred orientation will be evaluated.

What are the mechanical properties of the drawn steel wire? Such as hardness, Young's modulus, etc.

What is the relationship between composition, structure and mechanical properties?

What is the value of the residual stress of the drawn steel?

What is the impact of residual stress on the mechanical properties?

### **1.3 Objectives and Scope of the Present Work**

The high-carbon drawn steel has gained increasing interest because of their superior mechanical properties and has proved to be promising materials in many engineering applications. This project aims to explore the contribution of the microstructure and the orientation of the pearlite. Besides, the purpose is to understand why the final drawn has the best mechanical properties.

The result will give a deeper understanding of the controlling of microstructure and orientation on the mechanical properties and performances of the drawn steel. With the study on the residual stress and microstructure, one can understand the mechanical properties of the drawn steel from a different point of view. It will give a new concept to future drawn steel application.

## **CHAPTER 2 Literature Review**

### **2.1 The microstructure of the drawn steel**

J.Toribio and E. Ovejero did some research on the steel wires and gave some micrographs in Fig. 1. They cut the seven steel wires and mounted them to receive the metallographic which could reveal the pearlite microstructure. Firstly, they grinded and polished the mounted samples, then the etchant (Nital 2%) was used. Each cold drawing stage gave a micrograph and they performed an analysis of metallographic according to the acquired date. It is very clear that pictures a and c (the original hot rolled bar) have similar features in L and T sections (both are oriented casually). The last stage of drawn steel had very obvious differences between the two sections-L and T. In the L section, the colony of the pearlite is spindy and remarkably oriented in the drawing direction while the T section shows no preferential orientation. In addition, they gave a clear structure of the middle degrees of cold drawing [11].

### **2.2 The Picture from SEM**

Some researchers (Xiaodan Zhang and Andrew Godfrey) did some SEM pictures on the steel wires.

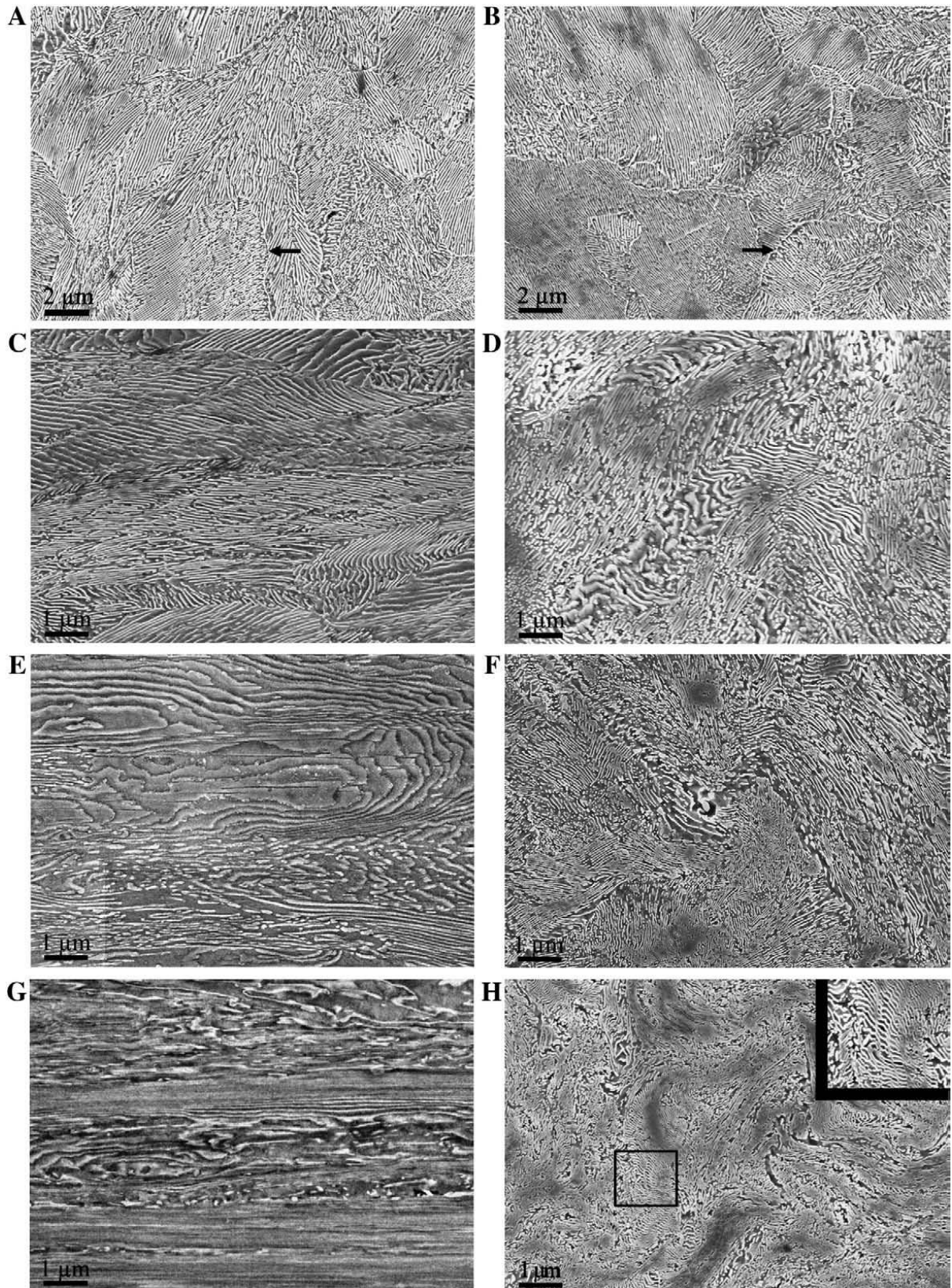


Fig 2.1 The SEM pictures from the longitudinal (A, C, E, G) and transverse sections (B, D, F, H) of the drawn steel wires in different strain:  $\epsilon=0$  (A, B),  $\epsilon=0.7$  (C, D),  $\epsilon=1.5$  (E, F) and  $\epsilon=2.7$  (G, H) [12].

Clearly, in the initial wire, the colony of pearlite has no preferred direction. Most of the cementite them are less than 4  $\mu\text{m}$  in length. Only 12% of cementite is larger than 4  $\mu\text{m}$ . The cementite sizes both in the longitudinal and transverse sections are in good concord. After the first time drawing, the strain becomes 0.7, the colonies of cementite have started to turn to the axis (the drawing direction). When the strain is 1.5, almost all of the cementite has turned to the drawing direction.

### 2.3 The lamellar deformation characteristics in drawn steel wires

After doing research on the process of drawing, Landford described the variation of microstructure in the drawn steel wires[13,14]. According to Landford, there are some severe distortions in the lamellar of pearlite and fibrous tissues in the cross-section after drawing. So, clearly, the cementite also indicates some ability about the plastic deformation from the conventional theory. In the pearlite steel, the cementite only makes up around 12.5%, but it is the strengthening phase. Therefore, the mechanical properties are closely related to the morphology and distribution of state of the cementite. So, many researchers have concentrated on the change of cementite during the process of drawing.

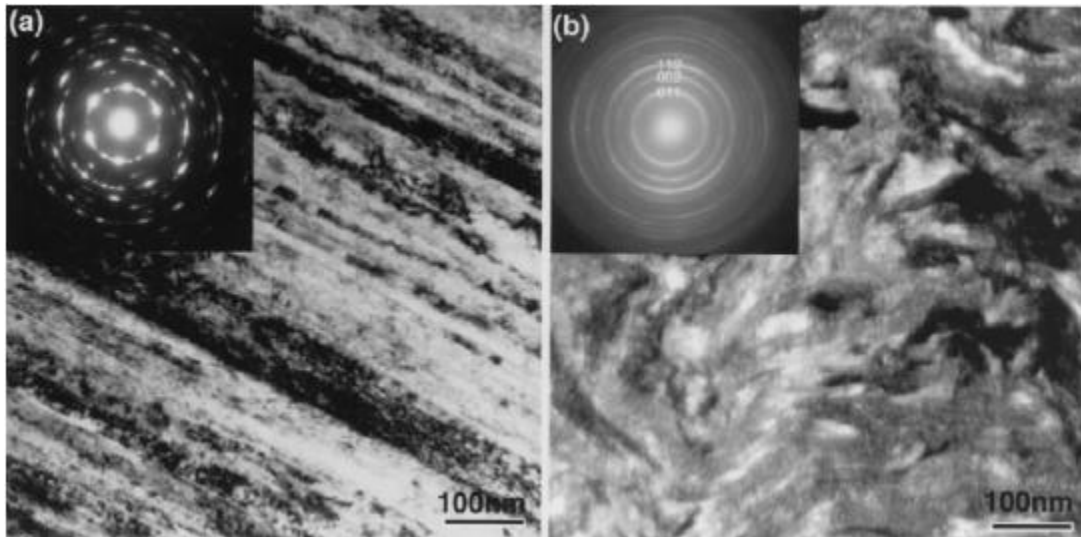


Fig 2.2 TEM micrographs and diffraction patterns obtained from the pearlitic steel wire [15]

Toribio, who argued the deformation way of cementite really depends on the angle between the orientation of lamellar and the drawing axis, did some work on the steel wires in

different strain [16]. Generally, there are three orientations of the pearlite interlamellar: the lamellars are parallel to the drawn direction, the lamellars are vertical to the drawn direction and there is an angle  $\theta(0^\circ < \theta < 90^\circ)$  between them. During the drawing process, the pearlite mainly received the tensile stress, which is parallel to the axis, and the compressive stress, which is vertical to the axis. According to the difference between the pearlite lamellar and the axis, the deformation mode can be divided into three kinds:

I—a certain angle between the interlamellar and the drawing direction

During the drawing process, under both the tensile stress, which is parallel to the axis, and the compressive stress, which is vertical to the axis, the deformation of pearlite interlamellar includes two aspects: the reduction of the lamellar spacing and the turning of lamellar orientation to the wire axis. When the drawing deformation strain is large enough, the direction of pearlite layers is almost parallel to the wire axis.(Fig. 2.3a)

II—the interlamellar parallel to the axis

Both the tensile stress and the compressive stress can reduce the lamellar layer. In this situation, the reduction has the fastest speed and the orientation of the pearlite is parallel to the axis all the time.

III- the interlamellar vertical to the axis

During the deformation process, the tensile stress from the axis would increase the lamellar spacing. However, the two ends of the pearlite layers receive the compressive stress which is perpendicular to the wire axis at the mean time, and the overall rotation is pretty difficult. Therefore, in this situation, the pearlite layer would gradually bend until the final fracture. (Fig. 2.3c)

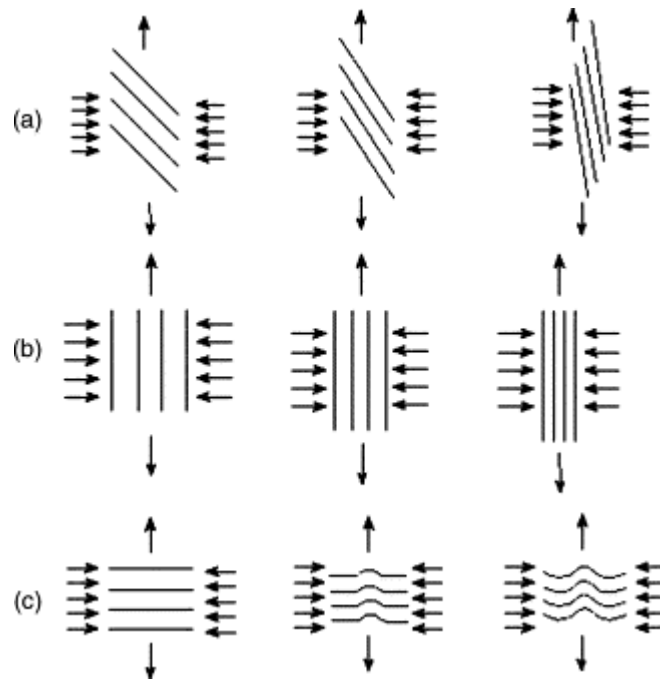


*Fig 2.3 Schematic diagram of pearlitic morphology change [16]*

## **2.4 The study on the cementite dissolution in the cold drawn pearlitic steel wire**

In recent decades, a lot of literature on the cold drawing steel wires with large strain deformation research have reported an important phenomenon [17-25]: at the room temperature, the strongly plastic deformation can make the large angle grain boundaries and the equiaxed grain in the size of 50nm-500nm, meanwhile, the second phase particles would go back to the melting phenomenon, then the matrix will become supersaturated solid solution again. In the following aging process, the second phase precipitates again the form of fine particles. This phenomenon has the universal significance in the alloy, therefore, a great number of scholars attached great importance to it.

After severe plastic deformation, the cementite layers in the steel wires are partially dissolved; many research results [17-25] have already confirmed the existence of the phenomenon. These studies mainly were used HRTEM (High Resolution Transmission Electron Microscopy), TAP (Tomographic Atom Probe), APFIM (Atom Probe Field Ion Microscopy) and Mossbauer spectrum analysis and so on.

In the earlier research, by comparing the Thermomagnetic curve the drawing, they discovered that the magnetization of the specimen occurred irreversible reduce above the Curie temperature of cementite, so it illustrates indirectly the dissolution of cementite after cold drawing. Talking about the pearlitic steel, the Mossbauer spectrum is made up by the spectrum of the ferrite and cementite, thus, we can calculate the cementite spectrum integral intensity to analysis the content of the cold deformation of cementite in the pearlite steel. Gavriljuk and etc. [17] used the Mossbauer Spectroscopy to analysis the changes of the cementite content in the cold drawing process. The result showed clearly that the cementite content decreases by 20% to 50% after drawing in the steel wires.

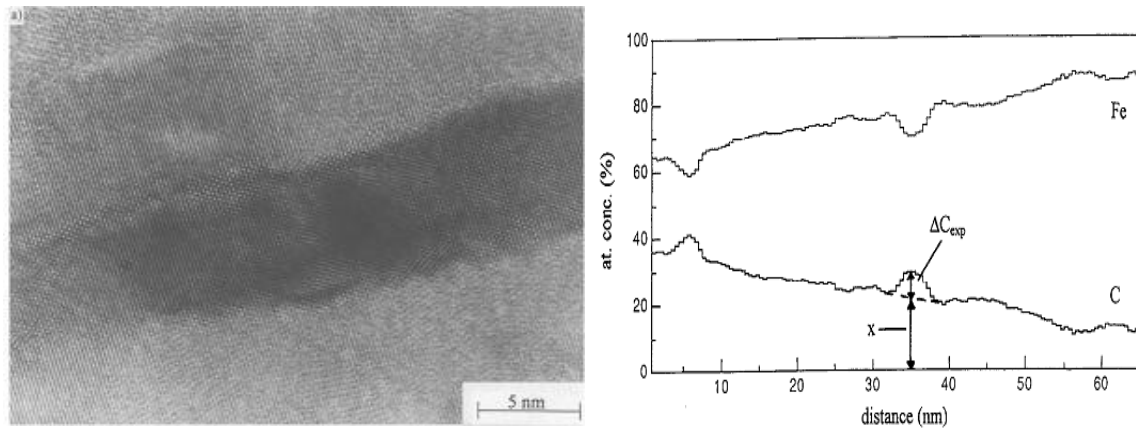


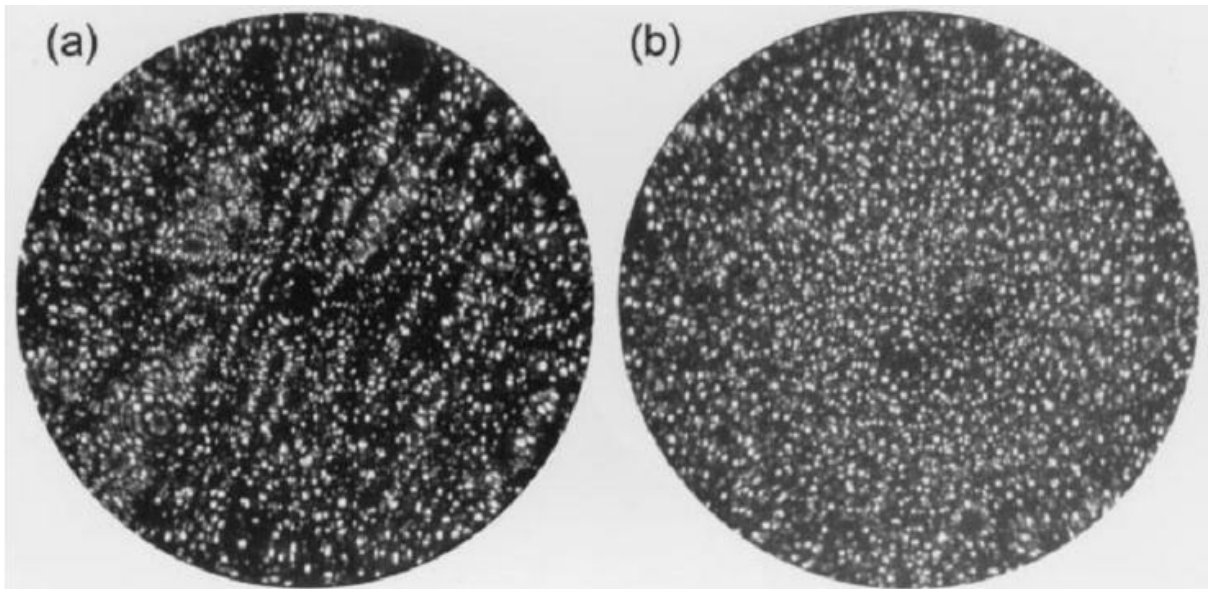
*Fig 2.4 Analysis of cold drawing pearlitic steel*

*(a) HRTEM micrographs in a lamellar zone showing adjacent ferrite lamellar*

*(b) Carbon and iron concentration profiles obtained in EELS[18]*

According to Languillaume, he used the HRTEM to observe the drawn steel wires after drawn, and he found that the adjacent ferrite lamellae is connected only through the interface (small-angle and large-angle grain boundary) without any presence of the cementite phase. He also used the EELS (Electron Energy Loss Spectroscopy) to analysis the samples, and he found that the concentration of carbon atoms go up and down in 7at.% to 11at.% in the original cementite region. (Fig 2.4) This range is much lower than the equilibrium cementite structure in carbon atom content (25at%). Therefore, the phenomenon of the dissolution of the cementite in the range of eutectoid steel wire after the cold drawing can be proved.

Hono [20] and etc. operated the APFIM and TEM to compare the structure and the distribution of carbon atoms in different variable strains with the carbon content of 0.97%. In the strain of 3.6(Fig 2.4a), it is clear to see from the figure that the carbon atoms are distributed along the lamellar basically. However, when the strain reaches 5.1 (Fig 2.4b), the figure of FIM shows that the carbon atoms evenly distribute and the lamellar cementite disappears, in other words, the cementite is dissolved totally. The authors used the TAP to measure the carbon content in the ferrite and cementite lamellae in different strains, the results shows the concentration of carbon atoms is about 10 at.% in the rich region of carbon, which is far less than corresponding equilibrium cementite percentage(25 at.%). That means the cementite has already begun to dissolve. In addition, in the strain of 5.1, the cementite basically has been completely dissolved. However, Hono, who analysed the diffraction peak (110) found that there is nothing changes in the lattice constant of ferrite. It means that rare carbon atoms solved in the ferrite lattice actually after the high-strain drawing in the pearlite steel wire. According to this, Hono guessed, the atoms would locate around the high-density dislocation of ferrite after the dissolution of cementite. Then, they give the direct evidence to prove this theory.



(a)  $\epsilon=3.6$  (b)  $\epsilon=5.1$  [19]

Fig. 2.5 Ne field ion micrographs of the pearlitic steel wires [21]

Ivanisenke [21] used the 3DAP to analysis the distribution of the carbon atoms, and the results showed that the carbon atoms located around the defects such as the stacking faults after the dissolution of the cementite. (Fig 2.5)

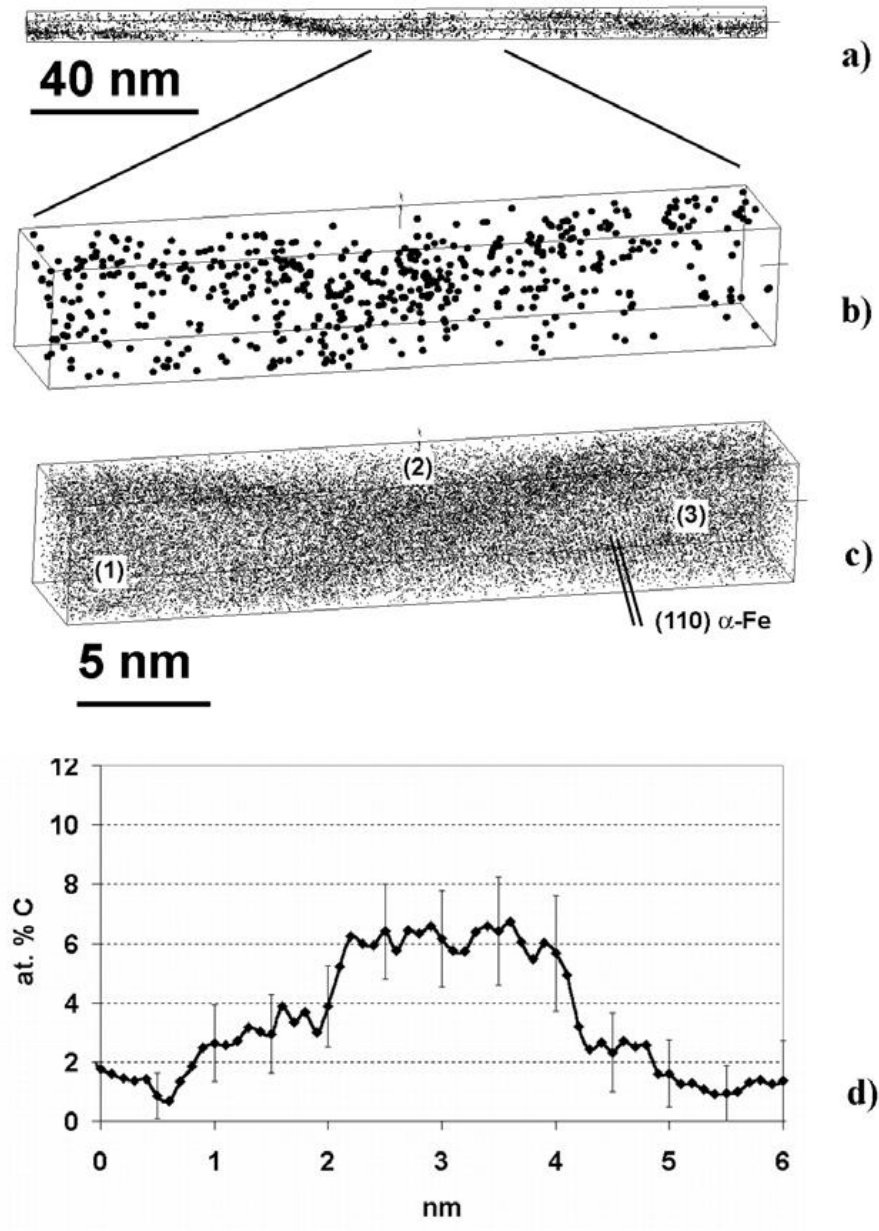
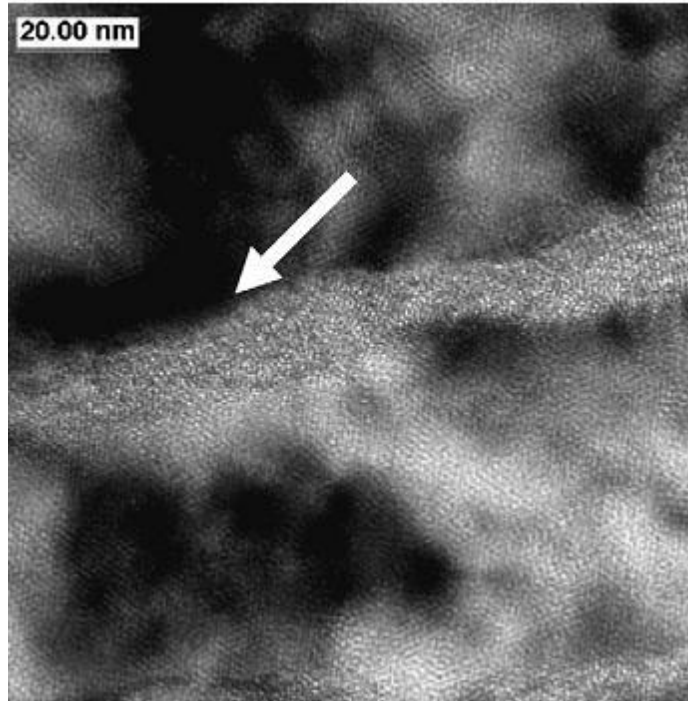


Fig 2.6 segregation of carbon atoms on planar defects as labelled 1, 2 and 3. [21]

Recent researches [22,23] show that, in the process of the cold-drawing, the severe fragmentation would happen in the cementite lamellae with the dissolution of the cementite, at the same time, there were some nanocrystalline and amorphous in certain areas of the

lamellae. The picture below shows the HRTEM micrograph of amorphous region in cold drawn wire (0.81C–0.20Si–0.49Mn–0.006P–0.008S (wt.%)). And the amorphous band is arrowed.



*Fig 2.7 HRTEM micrograph of amorphous region in cold drawn wire ( $\varepsilon = 3.6$ ) [23]*

## **2.5 The mechanism of the dissolution of the cementite**

In the conventional theory, the cementite lamellae in pearlitic are a hard and brittle phase which is generally difficult to have plastic deformation. By contrast, the dissolution of the cementite in the severe plastic deformation steel wires is a new topic in the day and age. Therefore, currently, there are few theories about the dissolution phenomenon in the cold-drawn pearlitic steel wires. At the moment, the researchers are concentrating on the study of the thermodynamics to explain the dissolution.

There are mainly two mechanisms as following:

### **2.5.1 Dislocation binding mechanism**

The cementite dissolution mechanism, proposed by Gavriljuk [24] based on the interaction of carbon atoms and dislocations, means the thermodynamic driving force for dissolution of the cementite from the carbon atoms and dislocation interactions can be greater than the binding energy for the carbon and iron atoms in cementite. Therefore, the

dislocation near the interface of ferrite and cementite would catch the energy from the broken keys of the cementite in the deformation process, which can lead to the cementite dissolution.

Basically, this mechanism is based on the following two experimental facts

According to the research, the enthalpy (0.78eV) between the carbon and the dislocation is larger than the formation enthalpy (0.5eV).

According to the experiments, some carbon atoms located around the dislocation and the slip planes.

This theory could explain the role of different alloying elements on the cementite decomposition. Through the internal friction methods, the binding energy can be measured between the ferrite and the dislocation which changes from 0.2eV to 1.8eV with the different alloying elements, and the decomposition enthalpy of the cementite is around 0.5eV [24-30]. Gavriljuk' work could show that the different micro-alloying elements can enhance and diminish the interaction between the effect carbon and dislocation. Also, he used this theory to explain the influence of alloying elements on the dissolution of cementite. For example, Ni can reduce the carbon and dislocation binding enthalpy to 0.2eV while Mn can increase to 1.76eV. That means Ni can keep the cementite stable while Mn can promote the decomposition of cementite. It is same with the result of the Mossbauer Spectroscopy.

In addition, the theory can explain the problem of the distribution of carbon atoms in the dissolution of cementite. When 20-50% of the cementite is dissolved, the carbon in ferrite would change from 0.2at% to 4.4at% [14, 31]. If those carbon atoms go into the ferrite crystal lattice, the lattice constant would increase. However, the XRD results show that there is no significant peak displacement. Nevertheless, if the dissolution of the cementite is caused by the binding mechanism of carbon atoms and dislocations, the excess carbon atoms would locate around the dislocation, which cannot cause the displacement of the ferrite diffraction peaks [32].

But this mechanism cannot explain the following questions:

According to Sauvage, who has done the research on the cementite decomposition in the pearlitic steel wire containing 0.7% Copper. In the case contains a small amount of copper, the cementite tends to be unstable and a part of the cementite lamellae starts to decompose under the low strain. Due to the low solubility of Cu in both the ferrite and cementite, most of

them locate in the grain boundaries, which have limited effect to binding energy of carbon atoms and dislocations. Therefore, it is hard to explain these problems by this mechanism.

Another research on the pearlitic steel wires containing martensite after cold drawing shows: even in the early stage of the deformation, the dislocation density is increasing slowly, but the cementite has already begun to dissolve [34].

Through the calculations, the concentration of carbon atoms is far less than the experimental value even counting by the maximum dislocation density.

### 2.5.2 The mechanism of interfacial energy

Languillaume [18] guessed that the cold drawing deformation can make the layers become thinner, and there were just a few important dislocations in the ferrite layers. The deformation caused the increase of the cementite interface energy, which leading to the Gibbs-Thomson effect and the dissolution of the cementite. Moreover, the carbon atoms would diffuse into the ferrite matrix. The Fig shows the estimated curve of the solubility of carbon in the ferrite under 300K.

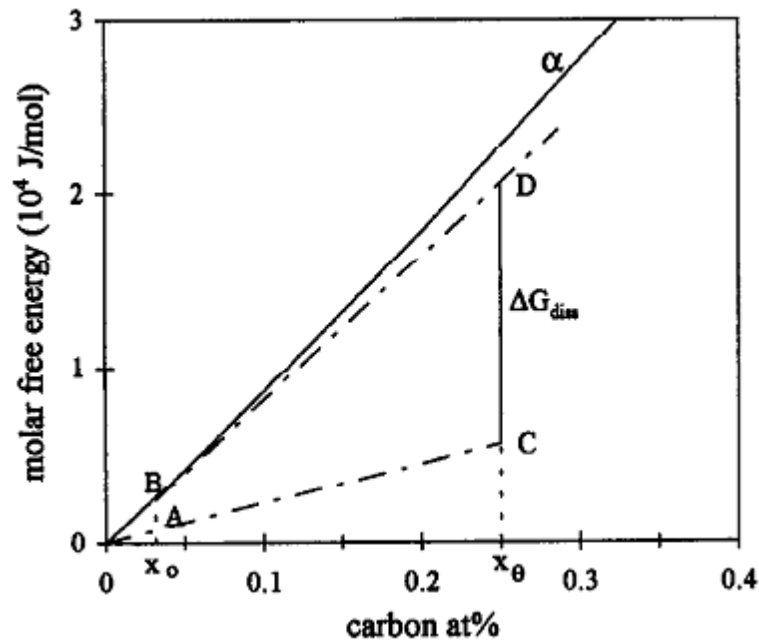


Fig 2.8 Free energy vs. composition for the ferrite-cementite system [18]

Creation of slip steps during the plastic deformation of cementite lamellae.

This theory can explain well that the cementite dissolves when there are not many dislocations in the ferrite. However, this mechanism cannot explain the internal friction test results, as talked above, since it cannot explain most of the alloying elements on cementite decomposition. Apart from that, this simplified model does not take into account the differences between the strain and the macroscopic strain of the cementite.

## 2.6 The change of the mechanical properties of steel wires

At the moment, there are few researches on the changes of the mechanical properties of steel wires caused by the dissolution of the cementite. According to Tarui [34] [35], he has done a lot of research on the change of the reversing performance caused by the dissolution of the cementite, found that as long as the cementite dissolution caused by the local concentration of carbon in the ferrite matrix containing more than 1 at. % after the cold drawing, it would lead to the occurrence of delimitation and then the reversing performance will decrease. Because the cementite dissolution leads to the local non-uniform distribution of the carbon atoms in the ferrite and thus strength of the ferrite is not equal. Prone to the local shear stress concentration in the lower local strength of the ferrite, the layered phenomenon happened when the wires are reversing.

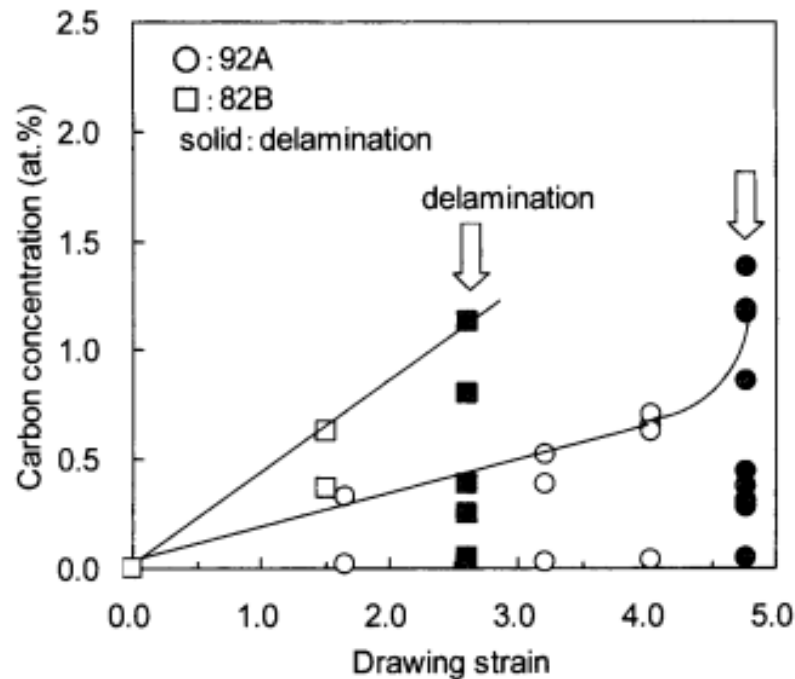


Fig 2.09 relationship between carbon concentration and the occurrence of delimitation [61]

## 2.7 The strengthening mechanisms of the cold-drawing pearlitic steel wires

At the first stage of the research, the study on the strengthening mechanism of the pearlitic steel wires mainly focused on the contribution of the lamellar spacing on the strength of the steel wires. A number of researchers [36-42] found that the pearlitic interlamellar spacing would gradually decrease as the increase of the strain. In addition, the yield strength of pearlitic steel wires with the cold deformation is similar to the Hall-Petch formula. They guessed that the obstacles from the cementite to the dislocation are same to the grain boundary, also, they pointed out that lamellar thickness of the cementite and pearlitic interlamellar spacing decreases as the cold deformation of the wire diameter decreases. Apart from that, the deformation of steel wires is axisymmetric during the process of cold-drawing. The wire strength conforms to the relationship of the hardening mechanism.

$$\sigma \propto k^{-1}\sqrt{S} \quad (2.1)$$

$\sigma$  the flow stress

$K$  the Hall-Petch coefficient

$S$  the pearlite interlamellar spacing

The Japanese researcher---Nishida[36] considers the hardening of the ferrite and cementite respectively in the drawing process. He also exploited rule to calculate the flow stress of the wire under a certain variable. Assuming that the ratio of two phases and the intensity of the cementite unchanged in the pearlitic steel wire drawing process, he was mainly caring about the hardening of ferrite. After that, the following relationship was obtained:

$$\sigma = V_{\theta}\sigma_{\theta} + V_{\alpha}\{\sigma_{\alpha 0} + (\sqrt{3}\alpha\mu b/S_{\alpha 0})\exp(B\varepsilon)\}$$

$\sigma$  : the flow stress after the deformation;

$\sigma_{\theta}$ : the hardness of the cementite;

$V_{\theta}$ : the volume percentage of the cementite;

$V_{\alpha}$ : the percentage of the ferrite;

$\mu$ : the elastic constants;

$b$ : the Burgers vector;

$S_{a0}$ : the original thickness of ferrite;

$\varepsilon$ : the drawing strain;

a, B: the constants;

Fig 2.11 is curves about the relationship between the drawing strain and tensile strength in the pearlite steel wires after different temperatures and isothermal transformation. The dashed lines are calculated by the hybrid rate. We can clearly see that when the strain capacity is small, the calculated curve and experimental curves will be coincided. However, when the dependent variable is greater than 2.0, the work hardening values calculated by the law of mixtures are lower than the experimental measured results.

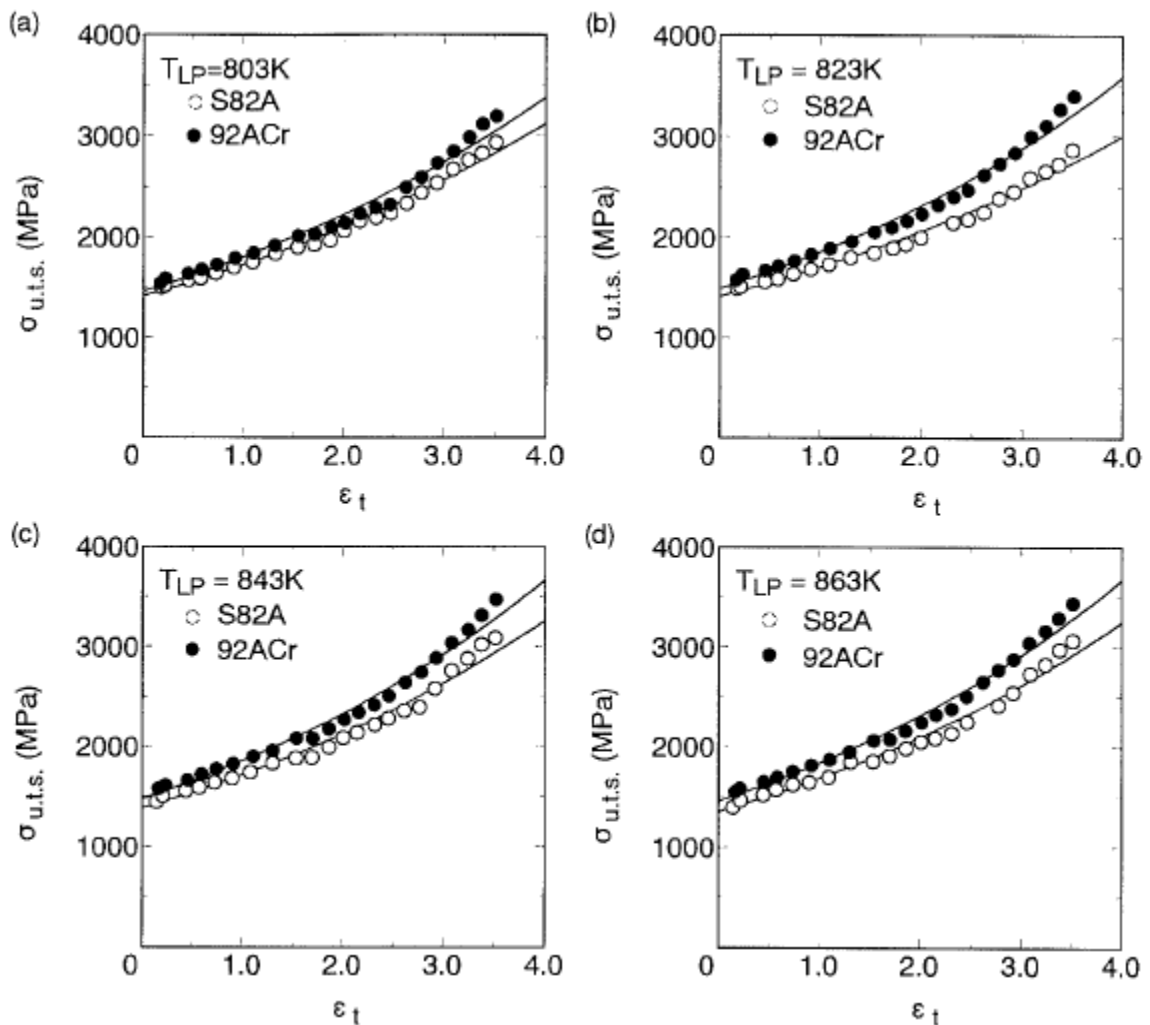


Fig 2.10 Effect of total strain on ultimate tensile strength of pearlite steel wires [36]

Taking into account the cementite during the plastic deformation, the eutectoid steel makes a large number of dislocations during the deformation at room temperature. We assume that the dislocations are making a decisive role in the wire strength. Langford [13] guessed that the cementite film shear stress should be inversely proportional to its thickness. Accordingly, he made the following relationship:

$$\tau_{\theta} = \tau_{\theta}^0 + 0.24G_{\theta}b_{\theta}(1/t) \quad (2.2)$$

$\tau_{\theta}$ : the shear stress;

$\tau_{\theta}^0$ : the lattice friction stress;

$G_{\theta}$ : the shear modulus of cementite;

$b_{\theta}$ : the Burgers vector;

$t$ : the thickness of cementite;

In recent years, there are some new progress for the large deformation of the organization in the cold-drawn steel wires, such as the dissolution of cementite [17-22] and the amorphous block [22, 23]. These structural changes provide new factors for the strengthening of steel wires. However, at the moment, people are paying less attention to the quantitative strengthen model.

## 2.8 The research content and significance

There are a variety of methods of severe plastic deformation, and large deformation of cold drawing is a very practical way to obtain large deformation, fine-grained high-strength materials, and industrial continuous production. With the development of modern manufacturing technology, the cold drawing speed and deformation of steel wire have been increasingly improved. Cold drawing is difficult to explain the dissolution of cementite in pearlitic steel wire with traditional theory. Therefore, in order to better promote the development of the industry, the need to develop the research of in-depth mechanism and process is urgent. In the previous study, the group has achieved some results in the evolution of the microstructure in the wire drawing process, the changes of mechanical properties and texture and residual stress evolution. However, it is still not adequate systematic study and discussion on the cementite dissolution phenomena in the cold drawn steel wire. Scholars in

this aspect both at home and abroad have made some progress, but there are still a few problems to be studied further. Here the author concludes the following four points:

After severe cold-drawing plastic deformation, the cementite in the pearlitic steel wire was dissolved compulsorily; the organization has undergone significant changes. The contribution of such changes on the wire strength cannot be explained by the traditional theory of layers of refinement to strengthen. The relationship between change and organizational evolution of the wire performance under large deformation is worth further study.

For cold drawing of the large strain conditions, a large number of studies have confirmed the compulsory dissolution phenomenon of cementite, but lack of quantitative analysis for it. The only proposed mechanism of cementite dissolution is also a number of thermodynamic models, lacking of research on the kinetic mechanism.

The changes of the supersaturated ferrite, which is formed after the dissolution of cementite in cold-drawn steel, in the subsequent heat treatment process and its impact on performance remains to be further study.

On the basis of the three points, it will be a quite practical problem how to control the processing conditions in the organization of the rod and drawing process, to get a good wire with higher strength, ductility and stability.

In view of the above problems, this thesis focuses on the more in-depth observational studies on the variation regularities of structure and property of the pearlitic steel wire in the drawing process.

The high-carbon drawn steel has gained increasing interest because of their superior mechanical properties and has proved to be promising materials in many engineering applications. This project aims to explore the contribution of the microstructure and the orientation of the pearlite. Besides, the purpose is to understand why the final drawn has the best mechanical properties.

The result will give a deeper understanding of the controlling of microstructure and orientation on the mechanical properties and performances of the drawn steel. The study on the residual stress and microstructure provides a different perspective to understand the

mechanical properties of the drawn steel from another point of view. This knowledge can give a new concept on future drawn steel application.

## CHAPTER 3 Approach and Methodology

### 3.1 General

In this project, all the samples were from hot-rolled wires which were made by the small die ( $\Phi 13\text{mm}$ ). All the samples were drawn continuously to different strains in the actual production line.

Element	Si	Mn	P	S	Al	Cr	Ni	Cu
Wt.%	0.30	0.70	0.009	0.003	0.006	0.190	0.020	0.050

*Tab 3.1 Chemical composition of samples*

In this project, the speed of the continuous drawing is 6m/s, and the rise temperature is around 150 °C; the discontinuous drawing speed is 3.8m/s each time, and the rise temperature is around 200 °C during the drawing. After the deformation, the microstructure and mechanical properties of the wires have significant changes, no matter the continuous drawing deformation or the discontinuous drawing deformation. In this chapter, we will start from the microstructure of the wires during the deformation process. Based on the previous research, this project will focus on observing the changes of pearlite especially the cementite. According to the changes of the mechanical property in steel wires, the relationship between the wire microstructure evolution and the mechanical properties during the process of drawing will be discussed.

Drawing pass	0	1	2	3	4
Drawing strain, $\varepsilon$ (%)	0	0.54	0.95	1.48	2.01
Diameter, $\Phi$ (mm)	11.50	8.78	7.15	5.50	4.20

Table 3.2 the samples details

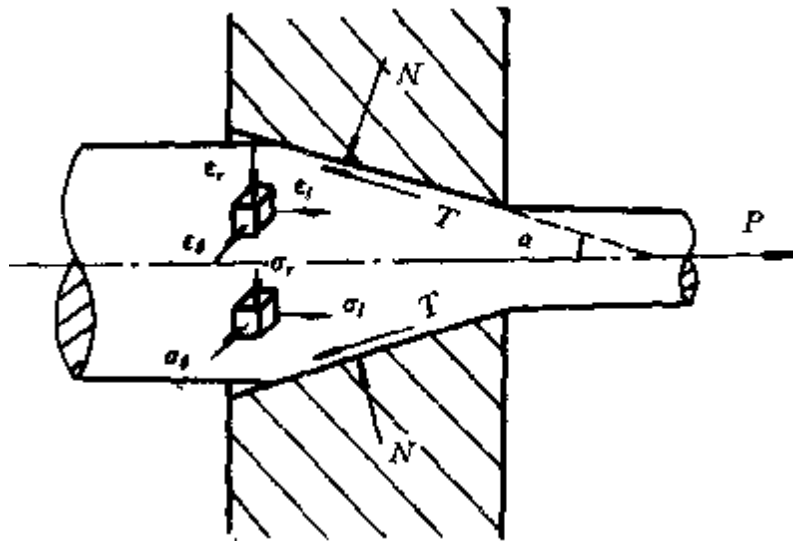


Fig 3.1 The schematic of the drawing process [43]

### 3.2 The research methodology

Taking drawn steel wires with different diameter as research objects, this project studies the composition, structure and mechanical properties of steel wires comprehensively with techniques such as XRD, XPS, SEM, nanoindentation

### 3.2.1 the metallograph

In order to know the microstructure of the five samples, the samples should be ground and polished and then etched by 4% Nital. Generally speaking, all metallographic laboratories are divided into three different basic areas: the specimen preparation area, the polishing, grinding and etching area, and the observation and photographic area.

The specimen preparation area: The sample preparation area must be equipped with some machines to cut or shear a metallographic specimen from the submitted piece.

The polishing, grinding and etching area: The area for polishing, grinding and etching must be free of dust totally. During this project, the grinding/polishing machine, made by Struers in Denmark, would be used. After the grinding and polishing, the samples would be etched by 4% Nital.

The observation/micrography area: In this area, a microscope should be equipped. In this experiment, a microscope made by Brunel Microscope LTD will be used to take the pictures of microstructures.

### 3.2.2 X-ray diffraction (XRD)

During this project, XRD will be used to characterize the steel crystallinity and phase structure of the drawn steel. In conventional  $\theta/2\theta$  configuration of XRD measurement, the penetration depths of X-rays are generally in the range of 10-100nm which is much higher than the thickness of most thin films. The substrate can give most information and the XRD can solve the problem successfully. Fig 3.1 has shown the schematic diagram.

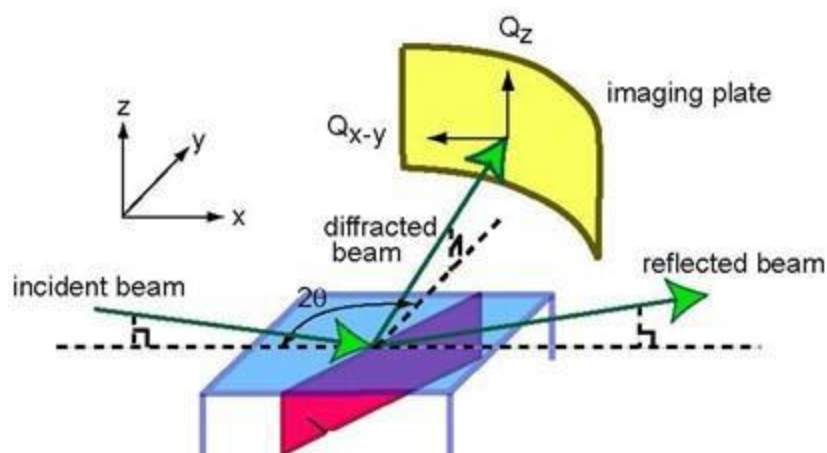


Fig 3.2 Geometry of XRD [43]

The distance between atoms or ions in materials, which allowing it to be diffracted within crystal lattice, is equivalent to the wavelength of X-ray. Thus, through this, XRD can give the information of phase structure, crystal orientation, lattice constant, grain size and some other related information of materials.

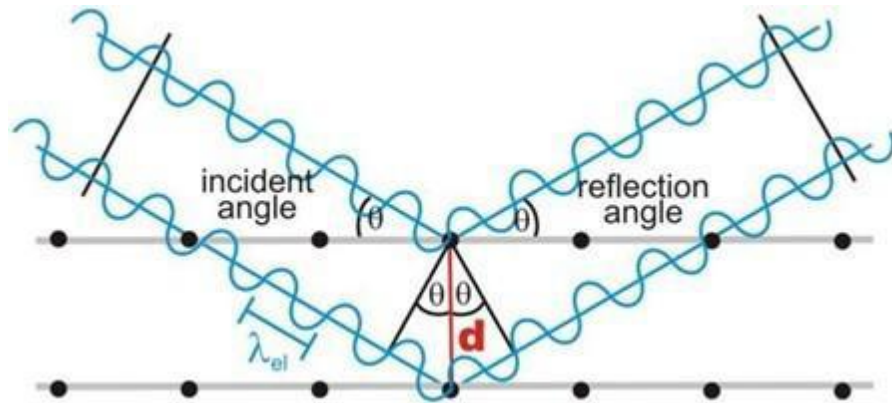


Fig 3.3 Interference of X-ray on atomic multilayer [44]

Fig 3.2 shows that when the optical path difference of adjacent atomic planes is equal to an integer multiple of the wavelengths, the scattered waves get interference and the reflection density is strengthened. In addition, the plane distance of interfered atomic planes should be a very famous formula which is known as Bragg's Law.

$$2d\sin\theta=n\lambda \quad (3.1)$$

In this formula,  $d$  means the spacing between atomic planes in the crystalline phase and  $\lambda$  is the X-ray wavelength,  $2\theta$  is the diffraction angle.

According to GuoZhong Cao [45], diffraction peak positions can be affected by homogeneous and inhomogeneous strains. There is another popular formula called Sherrer formula [46]:

$$D=\frac{C\lambda}{\beta\cos\theta} \quad (3.2)$$

In this formula,  $D$  is the crystallite size, and  $C$  is a constant related to crystallite. According to Sam Zhang and Nasar. Ali,  $C$ , normally equals to 0.91 [47],  $\beta$  is the peak width at half maximum of diffraction peak height, while  $\lambda$  is the incidence wavelength.

There is another function of XRD to measure the lattice parameters of the drawn steel. The following will give the formula:

$$a=(hkl) \sqrt{(h^2 + k^2 + l^2)} \quad (3.3)$$

Here,  $a$  is the lattice parameter,  $D$  ( $hkl$ ) is the interplaner spacing and ( $hkl$ ) is the crystal plane indices.

### **3.2.3 Focused Ion Beam (FIB)**

In this project, FIB (focused ion beam) will be applied, because this machine can observe the structure of the steel wire from the cross-section view. Moreover, it can prepare the samples for TEM imaging. This method has the ability to manufacture samples which cannot be produced by traditional ways.

According to M. Andrzejczuk [48], FIB has been widely used in semiconductor industries since 1987. Due to its high precision milling and good imaging contrast, it has gained broader applications in cross-section observations of drawn steels [49]. Besides, FIB and TEM can be used together to observe the deformation zone made by nanoindentation, thus the deformation behaviour of steel wires can be studied clearly.

SEM and FIB have different workstation: SEM uses electron beam, while FIB uses metal ion source (normally  $\text{Ga}^+$ ) to bombard the specimen surface, and secondly charged particles are detected to generate images [50].

By controlling the ion beam current, FIB can be used for two modes: milling and imaging. During the process, quick observations are preferred to reduce the surface damage. To protect the surface, a platinum layer will be deposited onto the coating before the milling process.

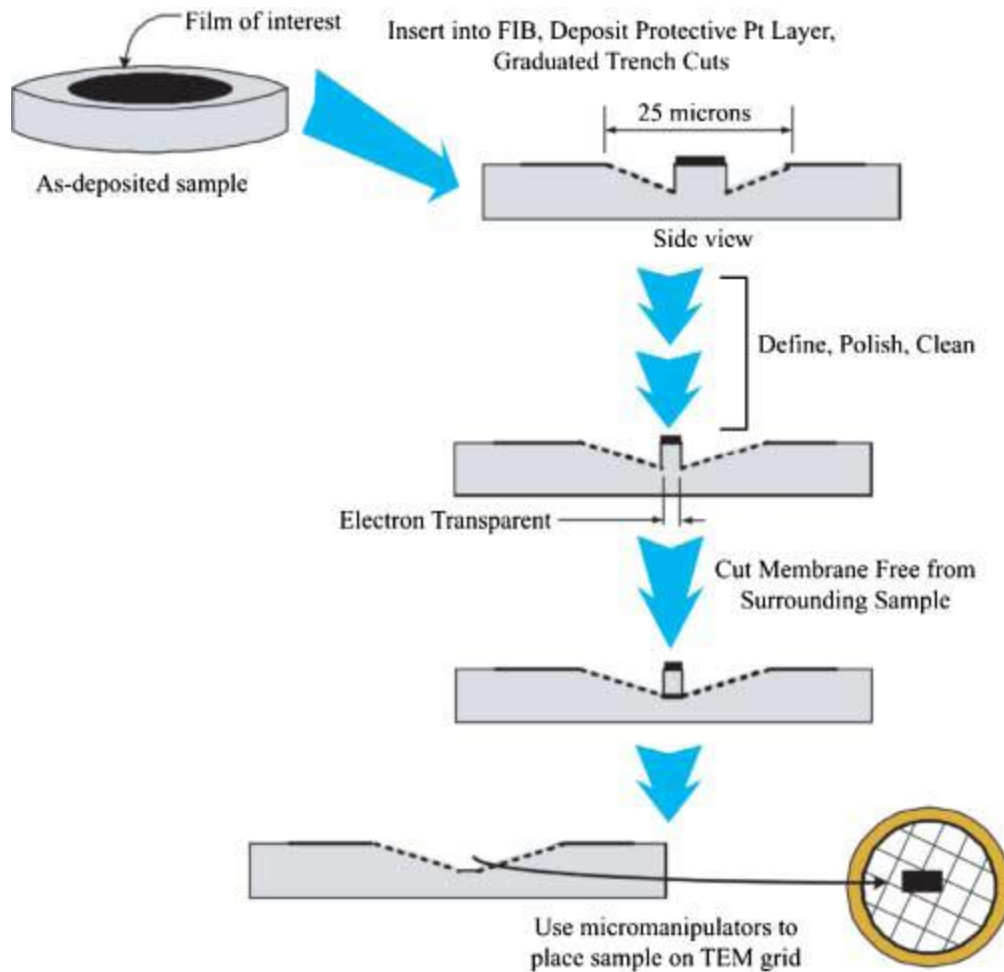


*Fig 3.4 Schematic of the lift-out FIB technique for a film on a substrate [51]*

In addition, during the TEM process, in order to obtain signal from the transmitted electrons, the thickness of the specimen is required less than 100nm which can be achieved by the FIB application. It is shown in Fig 3.3. This technique is called “H-type” technique because the specimen is like the letter 'H' when viewed from above angle [52].

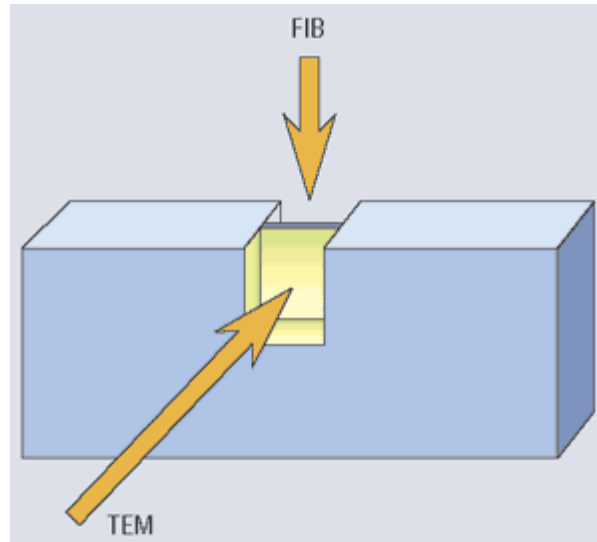


*Fig 3.5 TEM specimen prepared by FIB milling [53]*

### **3.2.4 Nanoindentation test**

In this project, mechanical properties of drawn steel wire will be measured by nanoindentation. Apart from mechanical properties, residual stress can also be tested.

Typically, the thickness of the steel wire is generally a few centimeters. It is very difficult to test equipments in traditional ways. At the moment, this problem can be solved as the appearance of the nanoindentation. Nanoindentation has been widely used in hardness testing of metal materials since the force range is a round mill-Newton.

Before the nanoindentation test, the surfaces of those samples should be ground and polished properly like the experiment in the metallograph. During the process, the contact area is determined by measuring the depth of penetration of the indenter into the specimen surface, thus, there is no need to make direct measurement of the contact area by optical microscope or even microscope with higher resolution.

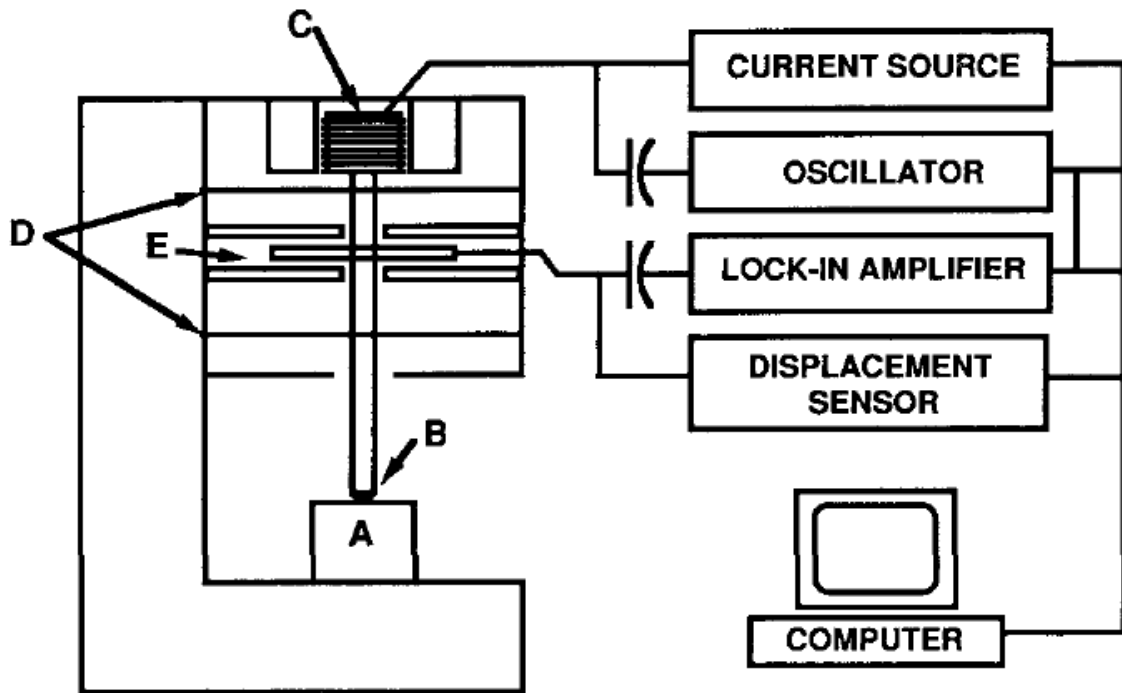


Fig 3.6 A schematic representation of the experimental apparatus used to perform the indentation experiments: (A) sample; (B) indenter; (C) load application coil; (D) indentation column guide springs; (E) capacitive displacement sensor [53]r.

During the process, the computer system can control the nanoindentation test automatically. The applied force on the specimen by either a Berkovich or spherical indenter can be controlled by a complicated feedback to ensure that the force is always correctly giving. The moving distance of shaft position can record the penetration depth. In Fig 3.5, the layout of the nanoindentation instrument is shown. A typical load-displacement curve is shown in Fig 3.6.

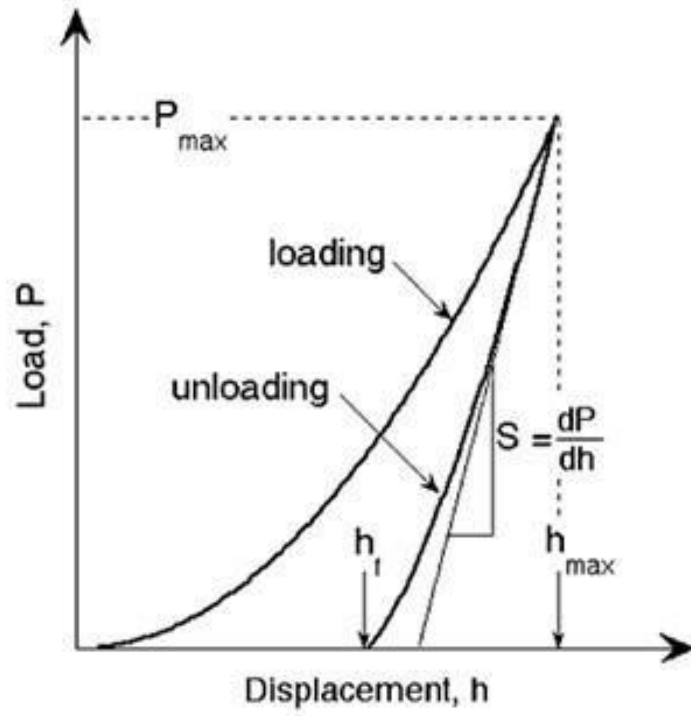


Fig 3.7 Typical load-displacement curve [53]

## CHAPTER 4 The Microstructure of Drawn Steel Wires

### 4.1 General

The wire forming is a cold drawn large deformation process. Its section compression ratio could reach up to 85%, and the carbon amount of most of the steel wire is more than 0.6%, with the strength up to 2000MPa after deformation. In the conditions of traditional production process, due to the lower drawing speed ( $<2\text{m/s}$ ), wire organization process conforms to traditional cold deformation theory. However, the speed of modern drawing production line is continuously towards high-speed development, with the  $10\text{m/s}$  maximum speed and  $15\text{m/s}$  or more in Japan, which has been further increased to 95% in pursuit of high-strength deformation compression rate. Thus, under the high speed and large deformation conditions (drawing speed of  $10\text{m/s}$  corresponding strain rate of  $5 \times 10^4\text{s}^{-1}$ ), both the material microstructure and the evolution of properties show various features not conforming to the traditional theories. In the new state, there are few systematic study and clear understanding of this problem, which influences the proposal of improvement measures on related process parameters including drawing speed, lubrication and mould design. This has limited the development of the steel wire products industry in some degree.

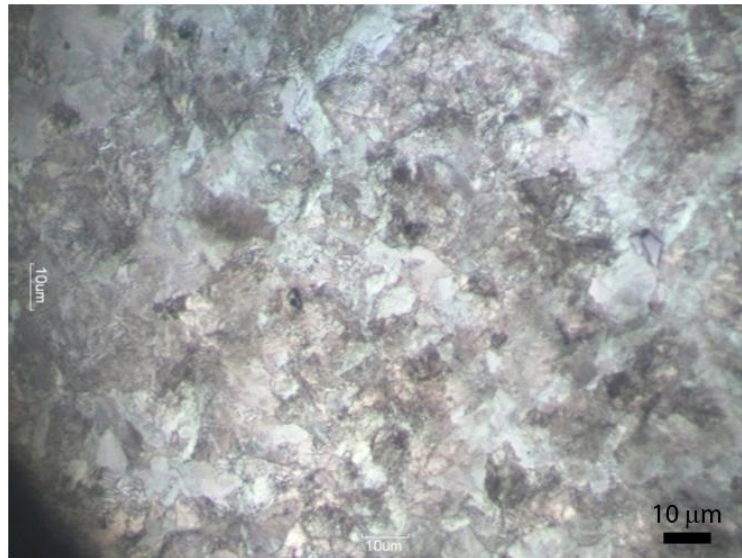
The eutectoid steel microstructure is composed of numerous pearlite conglomerates, the lamellae of adjacent pearlite conglomerates are in different directions. In the process of wire cold-drawing, macroscopically, with the diameter reducing the strength of steel wire keeps rising, and accordingly on the micro level the pearlite conglomerates go in fibrosis, the pearlitic lamellae is gradually turning to the parallel wire axis direction.

With the increase of the level of analysis, research on the tissue deformation during the pearlitic steel plastic deformation goes deeper. However, many aspects influencing mechanical properties of steel wire are still ambiguous, such as microstructure changes in the process of wire drawing deformation, the hardening characteristics of pearlite steel, etc.

This chapter is intended from the observation and analysis of the microstructure changes in the process of steel wire production, combining the mechanical properties of steel wire evolution, to probe into the hardening mechanism of pearlitic steel wire in the state of high-speed strain.

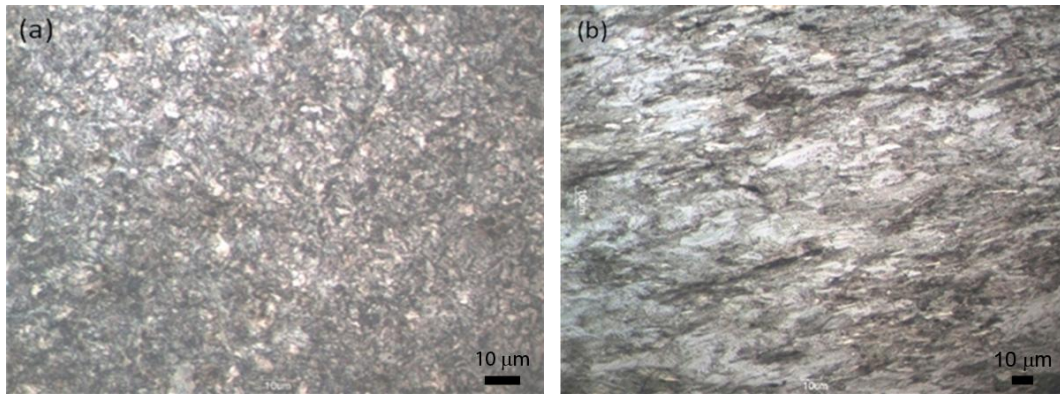
## 4.2 The metallographic analysis

Fig 4.1 is the metallographic photos of the original organization. It is clear to see from the picture that the typical sorbite organization and pearlier groups are small and equiaxed, and there are rare significant directions along with the vertical or horizontal. Also, there is little mesh precipitation of the ferrite in the grain boundary.



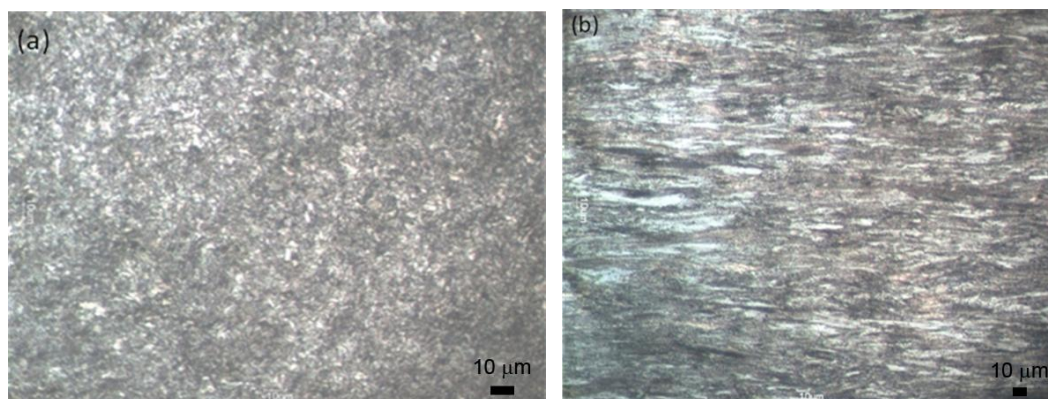
*Fig 4.1 the microstructure of the original wire*

Fig 4.2 shows the metallographic micrographs of the deformation after 2 drawing passes (i.e. from  $\Phi 8.78$  mm to  $\Phi 7.15$  mm, drawing strain of 0.95). It is apparent that the grains have been refined significantly in the transverse section. The grains have been considerably stretched in the longitudinal section.



*Fig 4.2 The microstructure of the drawn steel wire with a drawing strain of 0.95 (the deformation after 2 drawing passes): (a) transverse section, and (b) longitudinal section.*

Fig 4.3 shows the microstructure of the drawn steel wire after 4 drawing passes, with a deformation from  $\Phi = 5.50$  mm to  $\Phi = 4.20$  mm and a drawing strain of 2.01. As seen from Fig 4.3, the grains are further refined in the transverse section after more severe deformation. The microstructure of the drawn steel wire has clearly shown a fibrosis form in the longitudinal section.



*Fig 4.3 Microstructure of the drawn steel wire with a drawing strain of 2.01 (the deformation after 4 drawing passes): (a) transverse section, and (b) longitudinal section*

### **4.3 SEM observations**

Because the organizations of steel wires are very fine, it is difficult to observe the changes in pearlite interlamellar from the metallurgical microscope. As for the pearlitic steel near the eutectoid point, the mechanical properties are closely related to the distribution of

pearlite interlamellar. Therefore, the SEM has been used to observe the pearlite layer morphology in different strain, and the variation of the drawing deformation with the strain increasing was anglicised.

Fig 4.4 is the original organization SEM images of rolled wire rod. Clearly, this is the typical sorbite in eutectoid steel, and the pearlite colony size is around 5 to 10  $\mu\text{m}$ . The pearlite interlamellar is straight and there is no preferred orientation in the organization. The layer spacing is around 0.25 $\mu\text{m}$ . The grain boundary has no proeutectoid ferrite precipitation. It means that the control of the sorbite process is reasonable.

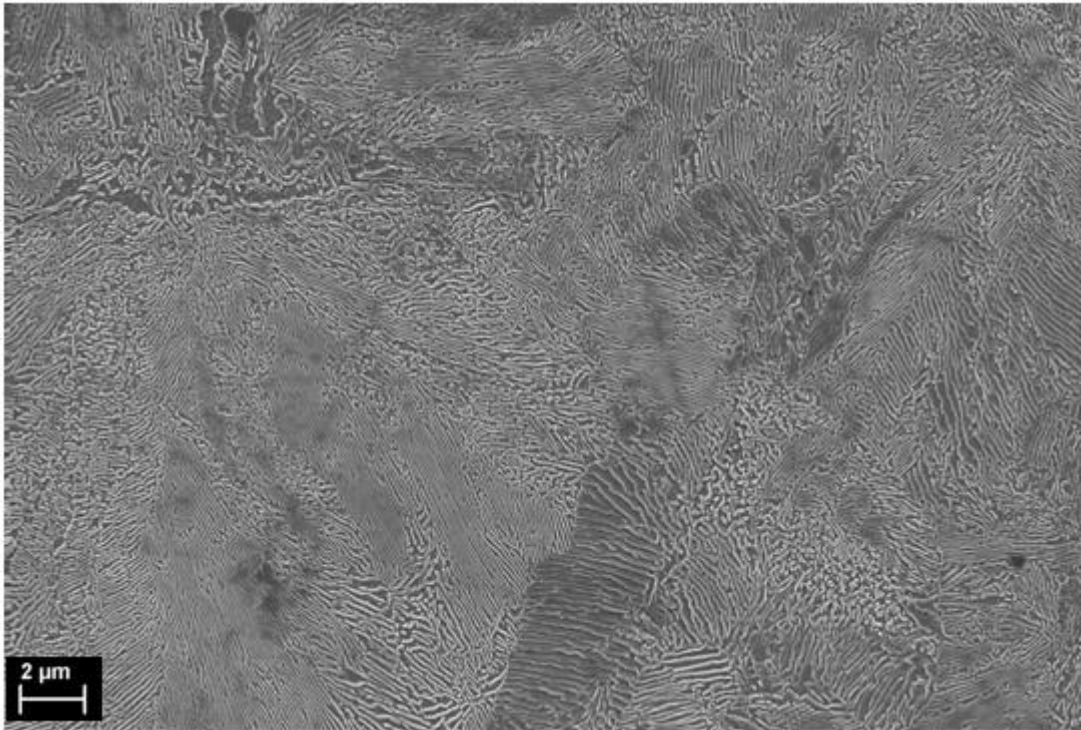


*Fig 4.4 Microstructure of wire before drawing*

Fig 4.5 is the pictures about the organization in cross section after drawing in different strain. According to the pictures, with the increasing of drawing deformation, the wire cross section of the pearlite interlayer spacing is gradually reduced. Apart from it, the pearlite layers are straight and flat before the deformation, while they gradually become curved after the drawing. In conventional theory, it is the plastic deformation of the brittle cementite phase under the radial pressure and the axial tension-stress.

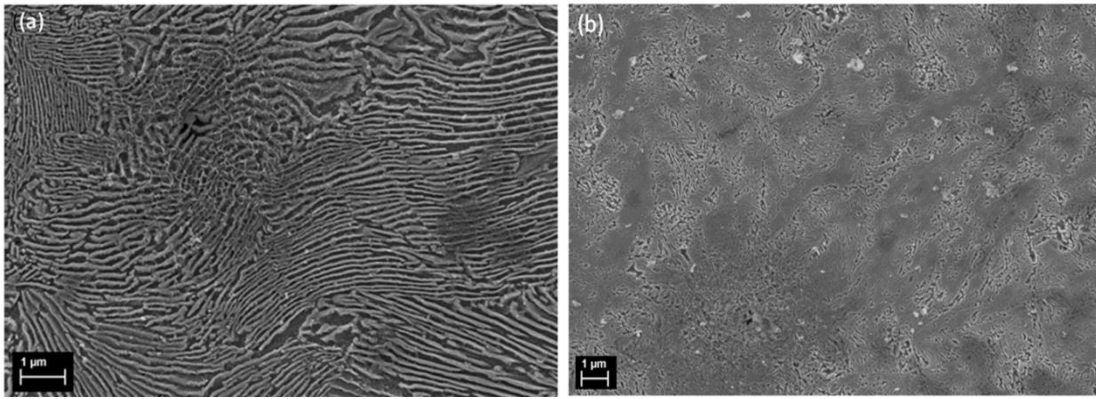


FIG 4.5 Pearlite morphologies in the drawn steel in transverse section with a drawing strain of: (a) 0.95, and (b) 2.01.

The Fig shows the pearlite microstructure morphology in long section in different strains ( $\epsilon=0.95, 2.01$ ). From the pictures, as the increase of the strain, cementite films gradually rotate to the drawing direction. When the strain reaches to the 2.01, all the pearlite layers rotate to the axis direction. However, there are some differences in the pearlite layers with the different original states. To be more exact, it is easy for the pearlite layers which are parallel to the axis originally to rotate, changing to the fibrous. In other words, it is quite difficult for the pearlite layers which are vertical to the axis to rotate.

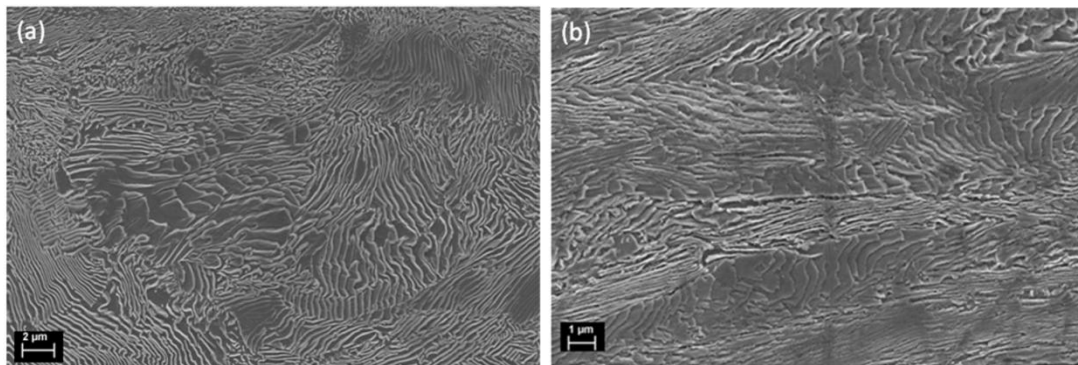
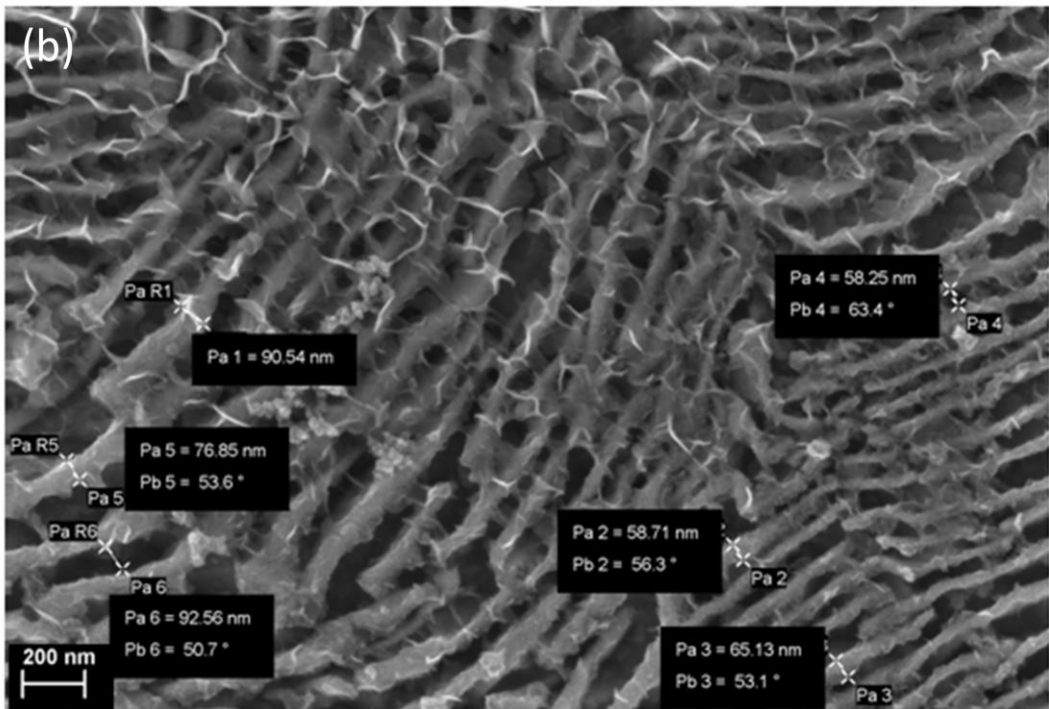
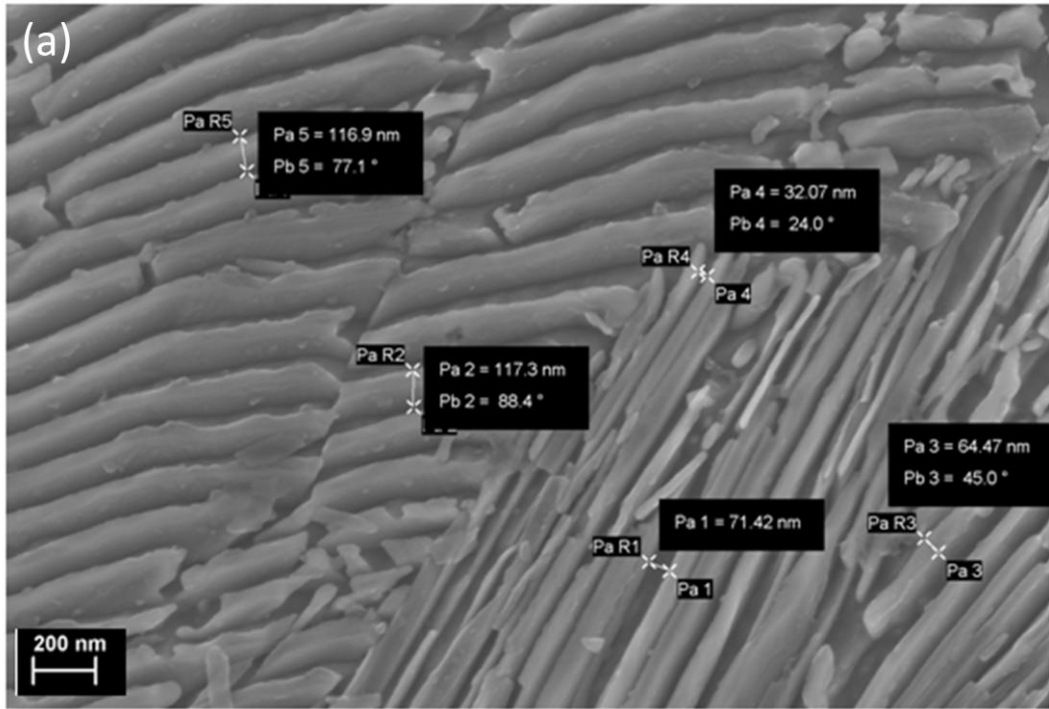


Fig 4.6 Pearlite morphologies in the drawn steel in longitudinal section with a drawing strain of: (a) 0.95, and (b) 2.01

#### 4.4 Lamellar spacing changes

From the previous observation, the pearlite group gradually adjusts to the arrangement along the pull-axis in the cold-drawing deformation process, and the layers refine slowly.

Pearlite interlamellar spacing is an important microstructure parameter of the mechanical properties in pearlitic steel wires. The pearlitic interlamellar spacing is the vertical distance between the two adjacent cementite and ferrite centre in a pearlitic colony. In this project, the lamellar spacing was measured by two vertical points in the SEM pictures (Fig 4.7)



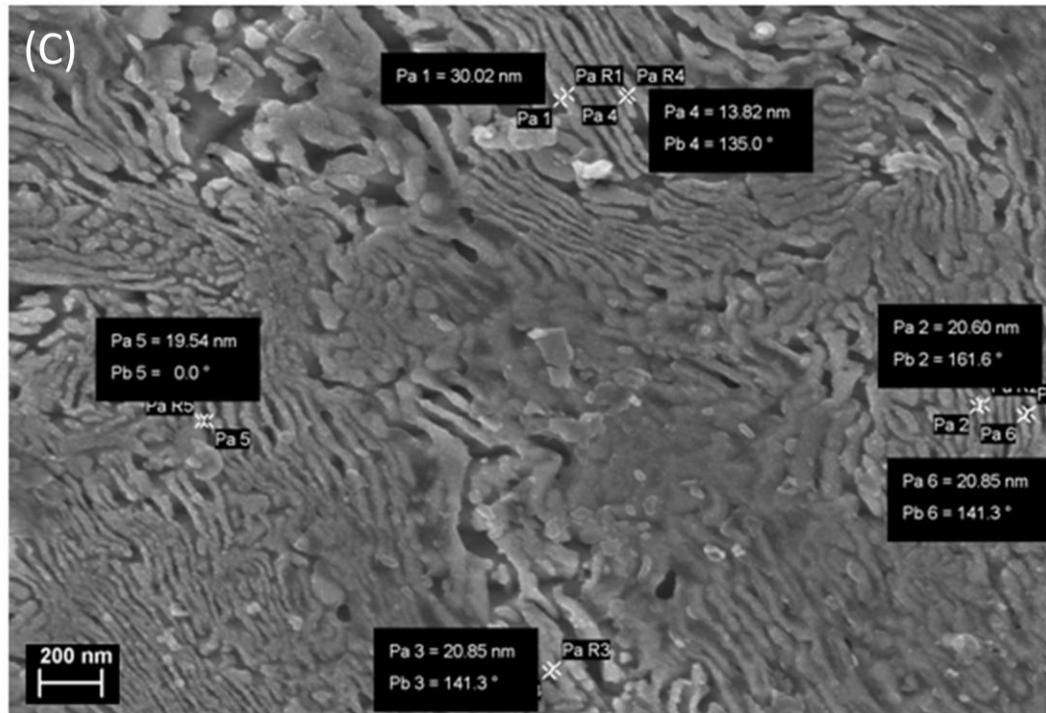


Fig4.7 the lamellar spacing

(a)  $\Phi=11.5$  mm (b)  $\Phi=7.15$  mm (c)  $\Phi=4.20$  mm

Obviously, pearlite lamellar spacing continuously decreases with the increase of the strain.

The assumptions of In S derived by literature is that initially all layers were ranked along the drawing direction.

The relation between yield stress and grain size is described mathematically by the Hall-Petch equation. According to measurements by SEM, the interlamellar spacing is following the Hall-Petch relationship.

In fact, the reduction speed of the pearlite inter-lamellar spacing during the process of steel wire drawing depends on the stress state of the film layer. And the stress is related to the layer's orientation. When the pearlitic lamellae approximately aligns along the drawing axis, the axial tensile stress and circumferential stress could cause the decrease of the lamellar spacing; in contrast, when the pearlitic lamellae orientation and drawing axis are in vertical direction, axial tensile stress will cause the increase of the lamellar spacing.

The previous observed results show: the orientation of pearlite lamellae is random in hot-finished rod; in the deformation of the initial stage, pearlite to drawing axial rotation; when the deformation reaches the extent that almost all the pearlitic lamellae are arranged axially along the wire, distinct changes will take place.

Therefore, in the process of drawing, with the changes of pearlite lamellar orientation, the decrease of pearlite inter-lamellar spacing is graded. Besides, as the deformation goes on, the reduction speed of the lamellar spacing will gradually increase.

## CHAPTER 5 The Mechanical Prosperities of Steel Wires

### 5.1 Hardness and Modulus from nanoindentation

#### 5.1.1 General

To measure the hardness and Young's modulus of steel wires, a Berkovich indenter of 5  $\mu\text{m}$  was applied, as shown in Fig 5.1, following Oliver and Pharr method [54] [55].

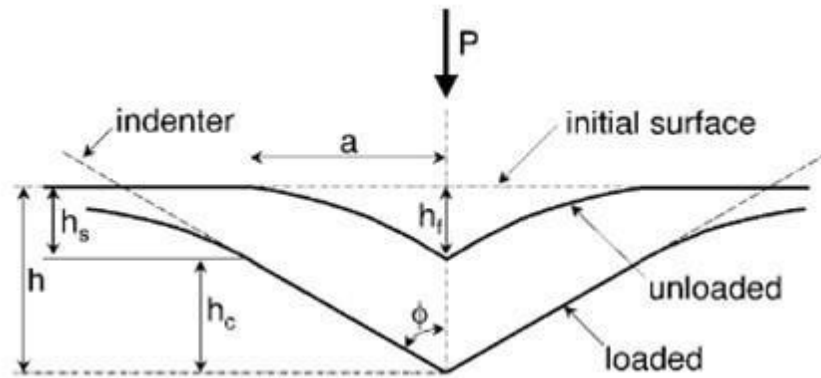


Fig 5.1 Schematic illustration of the unloading process showing parameters characterizing the contact geometry [54]

The deformation of hardness value ( $H$ ) can be expressed as:

$$H = \frac{P_{\max}}{A} \quad (5.1)$$

Where  $P_{\max}$  is the applied load and  $A$  is the contact area.

To calculate the contact area from the loading and unloading curves, the relationship between contact area,  $A$ , and penetration depth,  $h$ , should be clarified. The maximum depth is consisting of two parts:

$$h_{\max} = h_c + h_s \quad (5.2)$$

The sink-in depth,  $h_s$ , can be given by:

$$h_s = \varepsilon \frac{P_{\max}}{S} \quad (5.3)$$

Where  $\varepsilon$  is a constant that depending on the geometry of the indenter. For Berkovich indenter,  $\varepsilon=0.75$ .

Letting  $\varepsilon$  is a constant that depends on the geometry of the indenter. For Berkovich indenter,  $\varepsilon=0.75$ .

Letting  $F(d)$  be an “area function” that describes the cross sectional area of the indenter at a distance  $d$  back from its tip, the contact area  $A$  is then given by:

$$A = F(h_c) \quad (5.4)$$

The area function can be calibrated by independent measurements so that deviations from non-ideal indenter geometry are taken into account. These deviations can be quite severe near the tip of the Berkovich indenter, where some rounding inevitably occurs during the grinding process. Once the contact area is determined, the hardness is thereby determined.

The elastic properties of the indented materials can also be obtained from the unloading curve. The slope of the unloading curve is given by:

$$\frac{dp}{dh} = \frac{2}{\sqrt{\pi}} \frac{E^*}{\sqrt{A}} \quad (5.5)$$

The effective modulus  $E^*$  can be calculated as follows:

$$\frac{1}{E^*} = \frac{1-\nu^2}{E} + \frac{1-\nu'^2}{E'} \quad (5.5)$$

Where  $E$  and  $\nu$  are respectively Young's modulus and Poisson's ratio of the specimen, and  $E'$  and  $\nu'$  are those of the indenter.

### 5.1.2 Hardness

In this project, the hardness and Young's modulus were measured by the nanoindentation. The loads were 100 $\mu$ n, 200 $\mu$ n, 300 $\mu$ n, 400 $\mu$ n and 500 $\mu$ n.

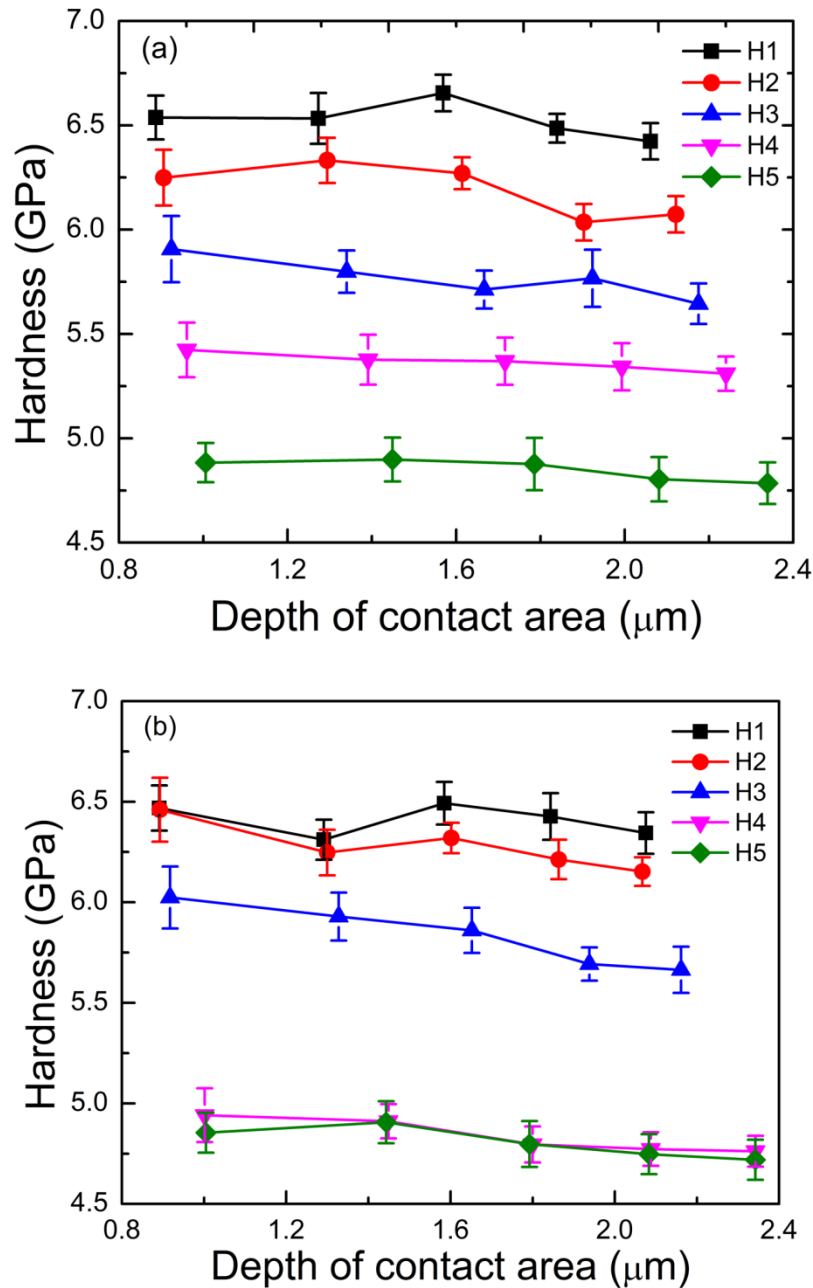


Fig 5.2 Hardness in the drawn steel wires in the (a) longitudinal section, and (b) transverse section: H1 ( $\Phi = 11.5$  mm,  $\varepsilon = 0$ ), H2 ( $\Phi = 8.78$  mm,  $\varepsilon = 0.54$ ), H3 ( $\Phi = 7.15$  mm,  $\varepsilon = 0.95$  mm), H4 ( $\Phi = 5.50$  mm,  $\varepsilon = 1.48$ ), H5 ( $\Phi = 4.20$  mm,  $\varepsilon = 2.01$ ).

It can be seen from the above pictures that the hardness increases remarkably as the increase of the drawing strain. Based on the above study, it is known that the hardness follows a Hall-Petch type of relationship with interlamellar spacing. Moreover, it can be seen from picture B (H4, H5) that the hardness improves slightly at the early stage of drawing. When the strain is small, the pearlite layers are randomly arranged. Under the axial and radial

compression stress, the layers which are parallel to the wire axis are easy to deform. The overall deformation is mainly from the pearlite colony coordination and the deformation of the pearlite layers. Therefore, the average pearlite interlamellar spacing decreases slowly.

### **5.1.3 Modulus**

The pictures show that there are no clear rules or changes in modulus in all kinds drawing wires. Young's modulus can be regarded as an index to measure the elastic deformation of materials.

Nanoindentation is relatively a new method to measure the hardness and modulus in metal. In future, this technology will be applied more in mechanical fields.

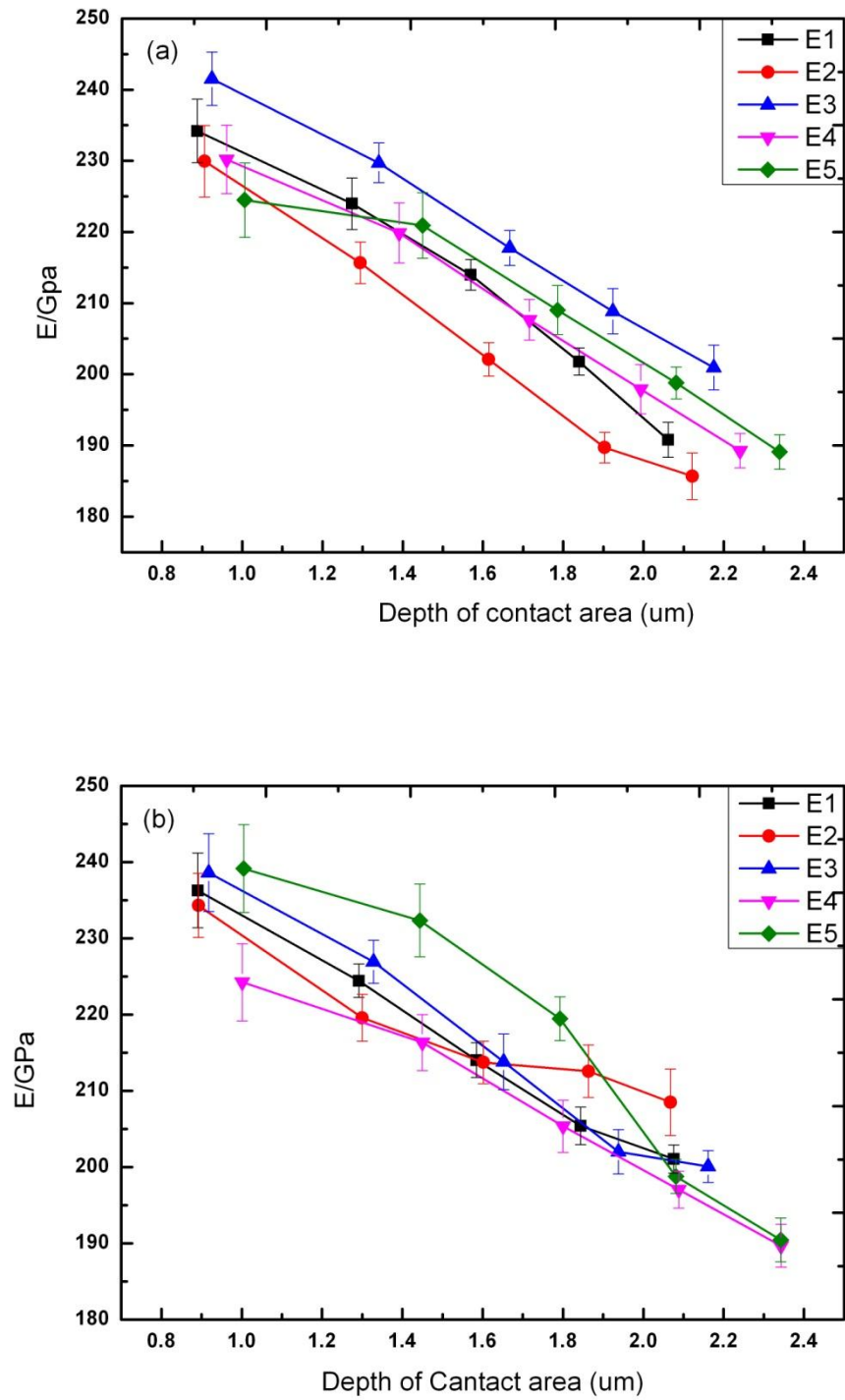


Fig 5.3 the pictures of modulus in steel wires

$a = \text{long section}, b = \text{cross section}$

(E1)  $\Phi = 11.5\text{mm}, \varepsilon = 0.$  (E2)  $\Phi = 8.78, \varepsilon = 0.54.$  (E3)  $\Phi = 7.15, \varepsilon = 0.95.$  (E4)  $\Phi = 5.50, \varepsilon = 1.48.$  (E5)

$\Phi = 4.20, \varepsilon = 2.01$

## 5.2 XRD

Based on the former study, around one third the cementite dissolves after the cold-drawing. Furthermore, the carbon atoms which are from the decomposition holds the average bond for 284.95ev which is higher than the bond of Fe-C.

In this chapter, the XRD was used to study the change of crystal structure happening during the drawing process. Although X -ray diffraction is not like the TEM, APFIM and other analytical tools which can react the internal microstructure morphology changes, its result can reflect the overall situation of the bulk samples.

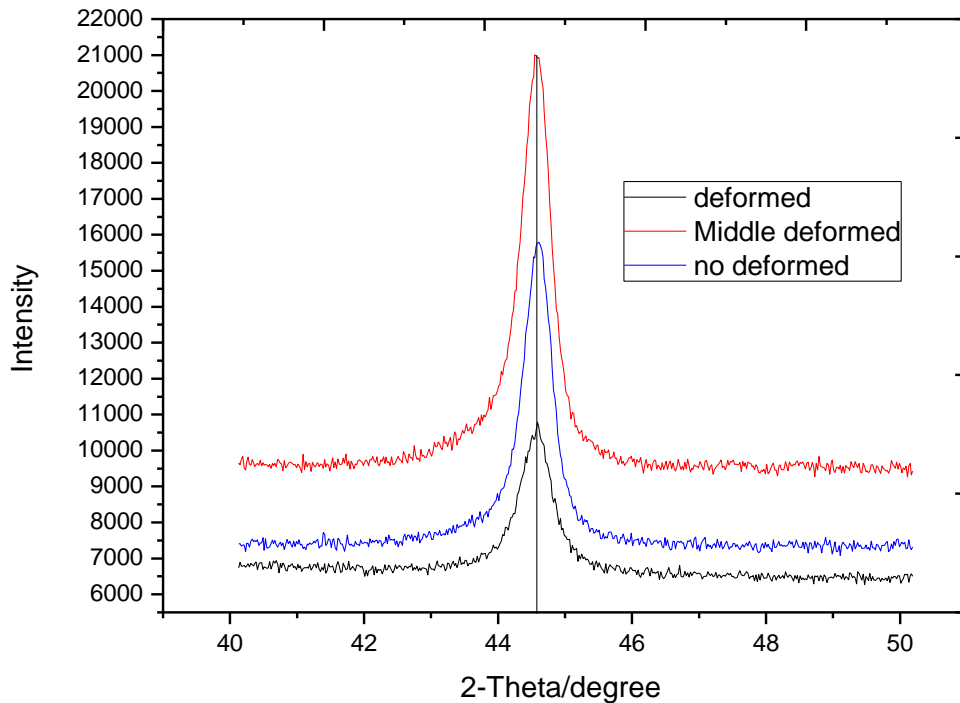


*Fig 5.4 XRD plot of  $\alpha$ -Fe {110} before and as-deformed in long section*

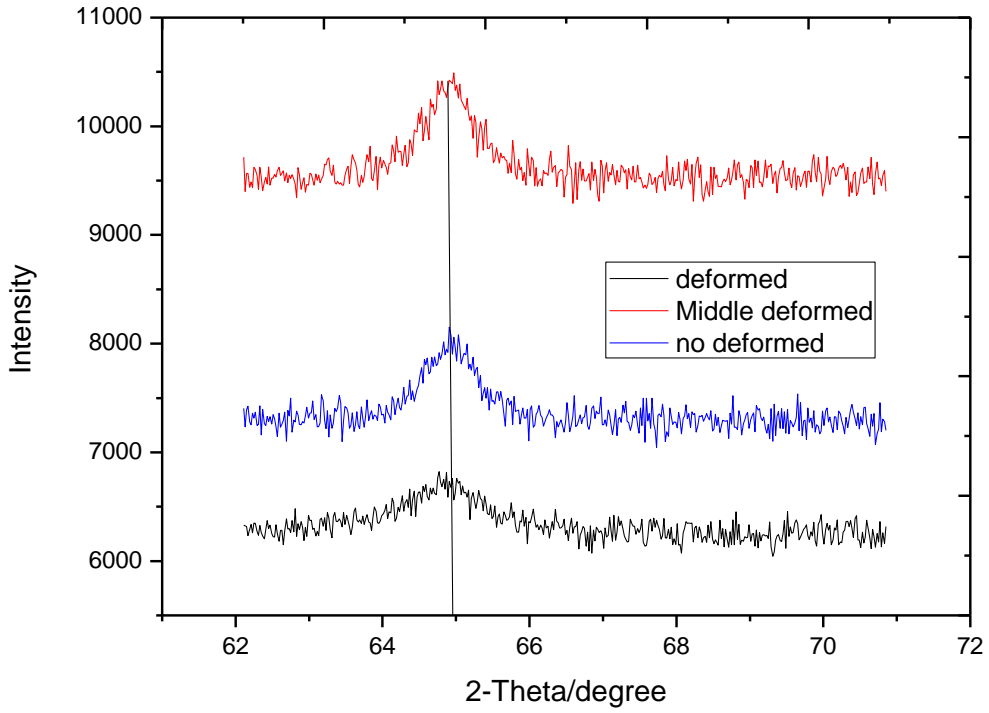


Fig5.5 XRD plot of  $\alpha$ -Fe {200} before and as-deformed in long section

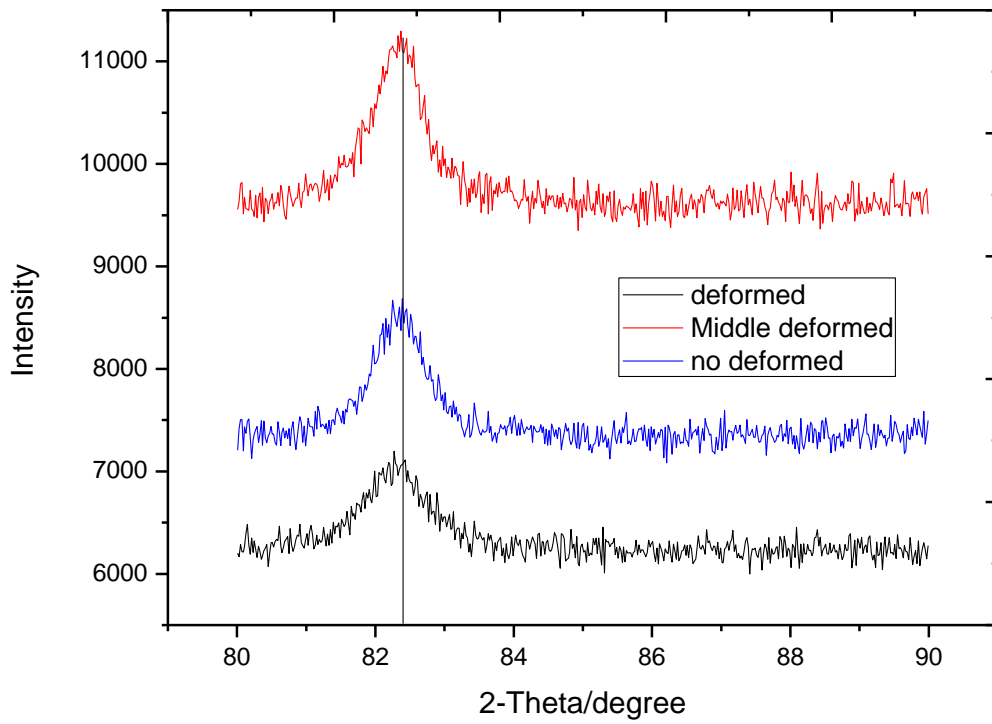
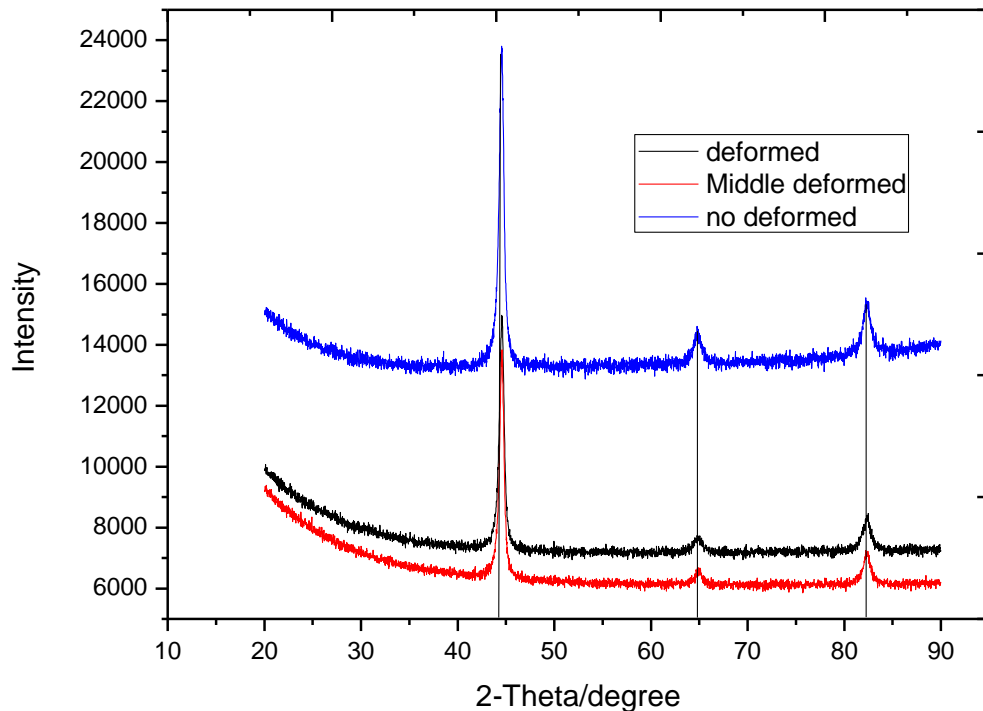


Fig 5.6 XRD plot of  $\alpha$ -Fe {211} before and as-deformed in long section

XRD were operated to analysis the phase change in steel wires before and after cold-drawing. According to the pictures, it can be seen that lines are similar in shape before and after deformation. The diffraction peak of ferrite becomes wide to some extent. This is probably due to the refinement of the ferrite layers and the increase in dislocation density in the layers. The diffraction peaks of ferrite do not change significantly. The picture below will indicates this problem.



*Fig 5.7 XRD plot of  $\alpha$ -Fe before and as-deformed in cross section*

### 5.3 Conclusion

In this chapter, a new research method (nanoindentation) was used the mechanical properties-hardness and Young's modulus. According to this, we can see that the mechanical properties increase obviously. Apart from that, XRD was used to study the change of ferrite lattice morphology.

## **CHAPTER 6 Microstructure from FIB**

### **6.1 General**

The structure of Focused ion beam is similar to the scanning electron microscopy, and the ion beam has replaced the electron beam. The detector would detect the secondary ions or the secondary electron after the ion-beam bombarding the surface of the sample. After that, the device will generate the maximum magnification up to 100.000 times secondary ion pictures. And this kind picture has excellent depth of field. Therefore, it is very suitable for accurate selected region of the sample surface to be processed.

The ion source of focused ion beam is used for Gallium ions. The reasons can be divided into two parts: (1) the gallium has low melting point and it is the liquid in the room temperature which is easy to facilitate to the gallium ions; (2) the Gallium can be focused into a small ion beam. Liquid gallium flow to the tungsten tip connected with the liquid gallium storage. Under the strong electric field of separation, the liquid is ionized into a gallium ion beam.

### **6.2 FIB Pictures**

In this project, the FIB was used to cut the surface of the steel wires. Then, the SEM can take pictures from the internal part.

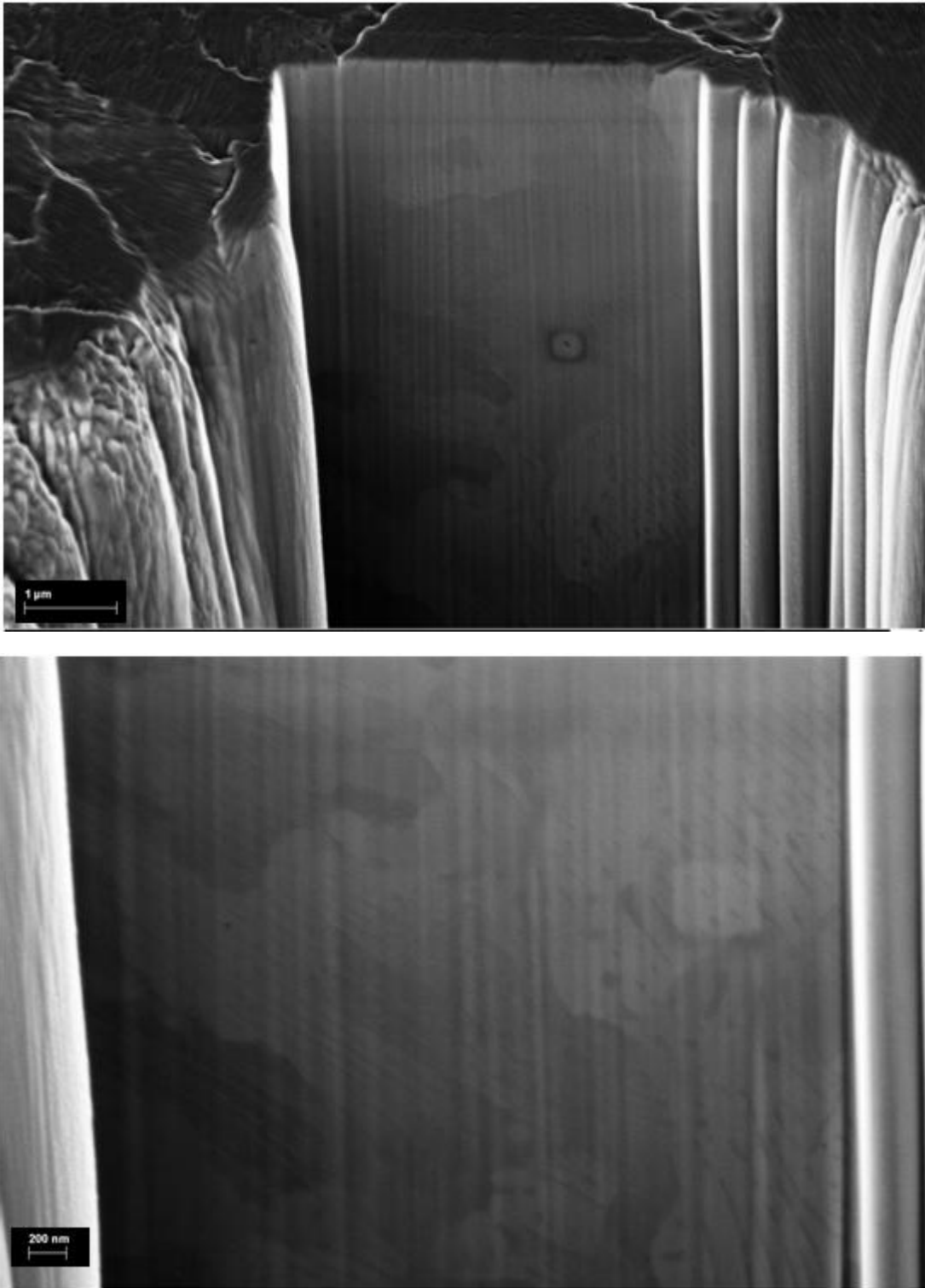


*Fig 6.1 the SEM pictures after FIB cutting from the original steel wires*

The pictures show that the microstructure is still in the initial state before the drawing.

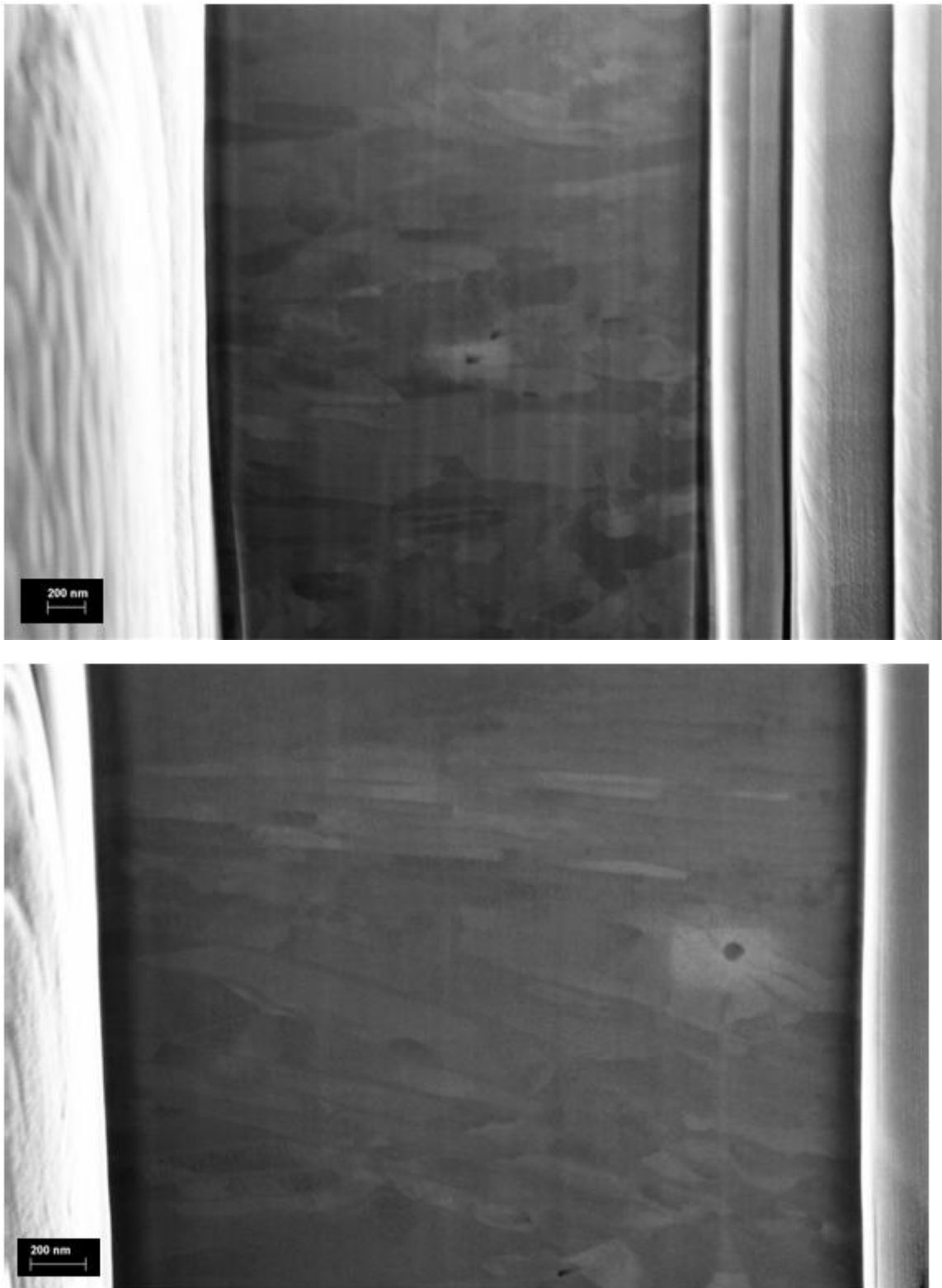


*Fig 6.2 the SEM pictures after FIB cutting from the Middle-deformed steel wires*

According to the above pictures, the structure has already begun to rotated to the drawing direction after drawing two times.

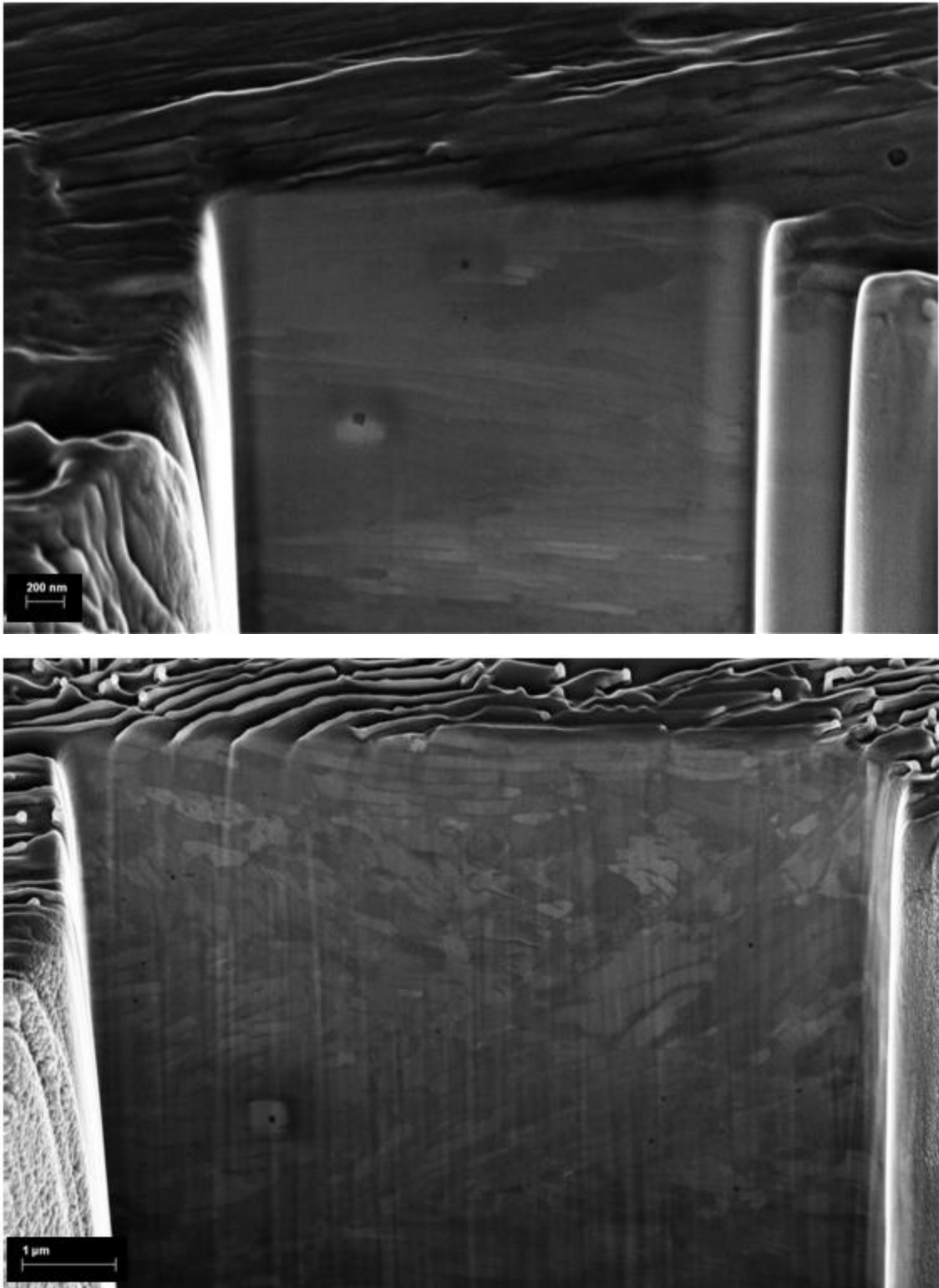


*Fig 6.3 the SEM pictures after FIB cutting from the deformed steel wires*

After the whole process of drawing, the microstructure is refined, changing to the axis direction.

In this chapter, FIB was used to cut the surface to take the pictures from the internal side of the wires. By doing this, the above research can be corresponded.

# **CHAPTER 7 The Stress-Strain Curve From Nanoindentation and The Modelling for The Steel Wires**

## **7.1 The stress-strain curve**

As talking before, the nanoindentation is a relatively new method to measure the mechanical properties. In this project, we used this device to generate the hardness and modulus. Apart from that, there is another important function of this device--- measuring the stress-strain curve.

As we all know, the stress-strain curve is extremely important graphics to describe the mechanical properties. It is the relationship between the stress and strain that a particular material displays.

Li H.he and Michael V. Swain did much work to investigate the stress-strain response of different dental materials, especially dental brittle materials and compared them with enamel. Here, in this chapter, the similar way was used on the samples with different strain to generate the stress-strain curve.

During the project, spherical indenter was used [Fig 7.1] to intent the surfaces of steel wires, loading from 100un to 500un. The gap between two indents on the samples was more than 50um to decrease the effects of residual stresses from other impressions.

\

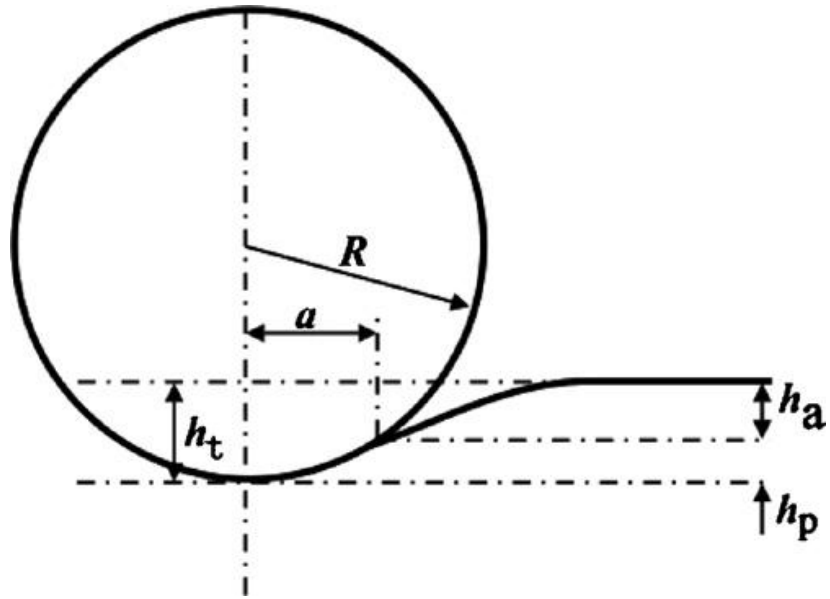


FIG7.1 Schematic illustration of contact between a spherical indenter and a flat specimen [56]

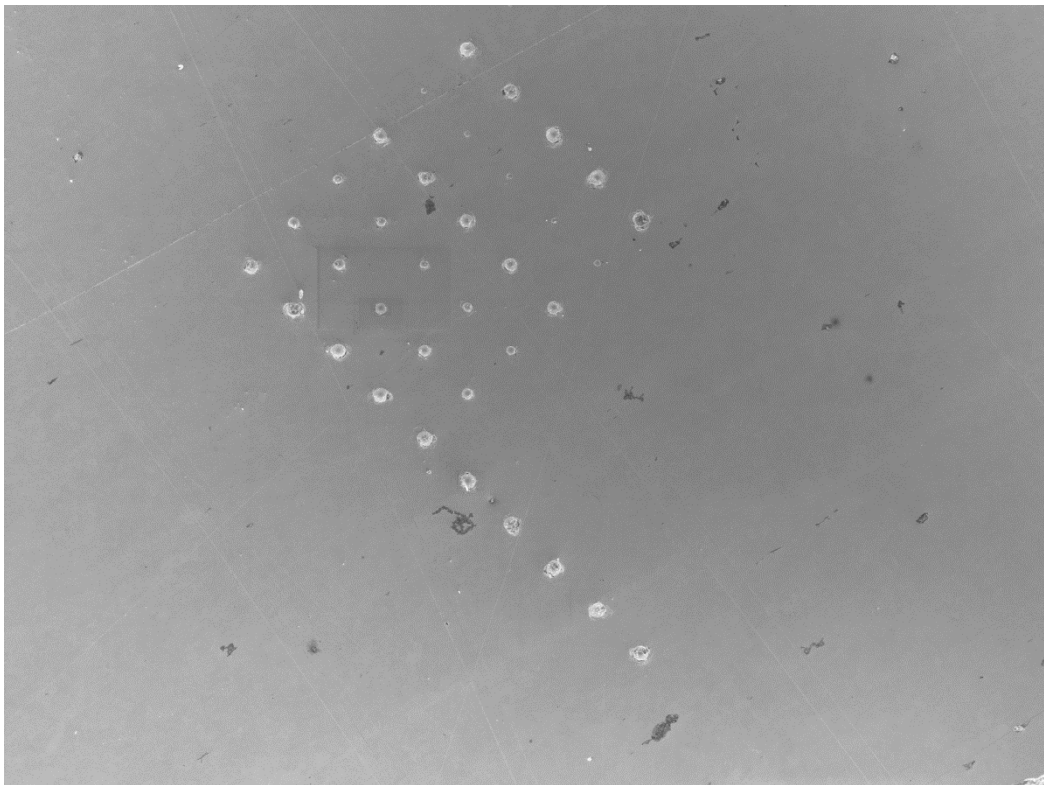


FIG7.2 the SEM pictures for the loading intents

By this method, the drawing for stress-strain curve is divided into two parts. Firstly, the straight line can be drawn by the modulus measured above, because the slope of the line is same to the modulus. The second part can be drawn by this new method. According to Li H. He and Michael V. Swain, the hardness divided by 3 is yield point. In addition, the strain can be generated from the  $a/R$  (divided by 5).

The relationship between the stress and strain that a particular material displays is known as that material's Stress-Strain curve. It is unique for each material and is found by recording the amount of deformation (strain) at distinct intervals of tensile or compressive loading (stress).

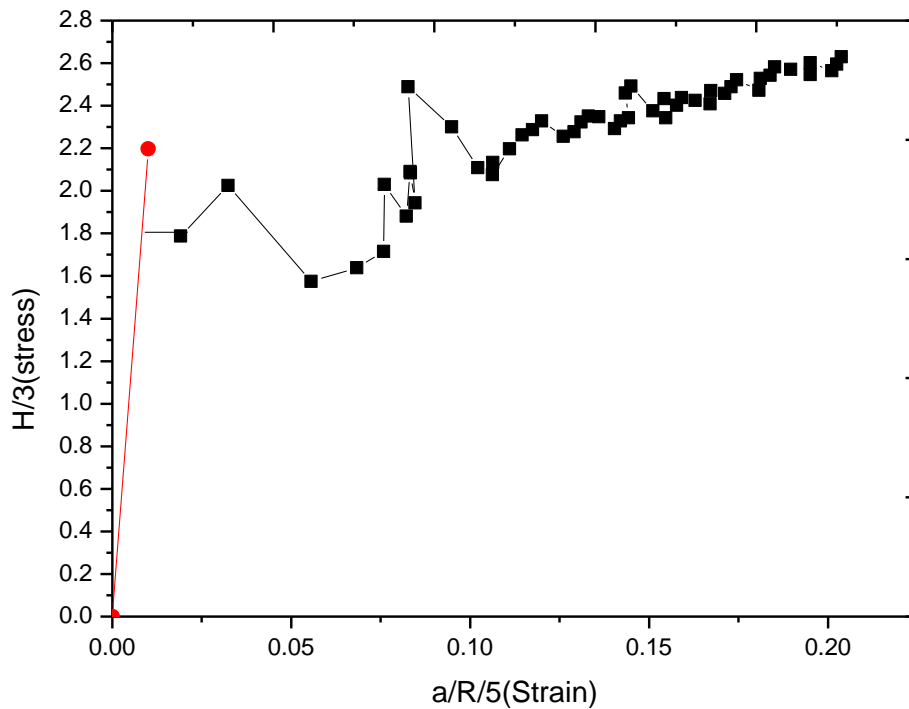


FIG7.3 the stress-strain curve from nanoindentation after the deformation

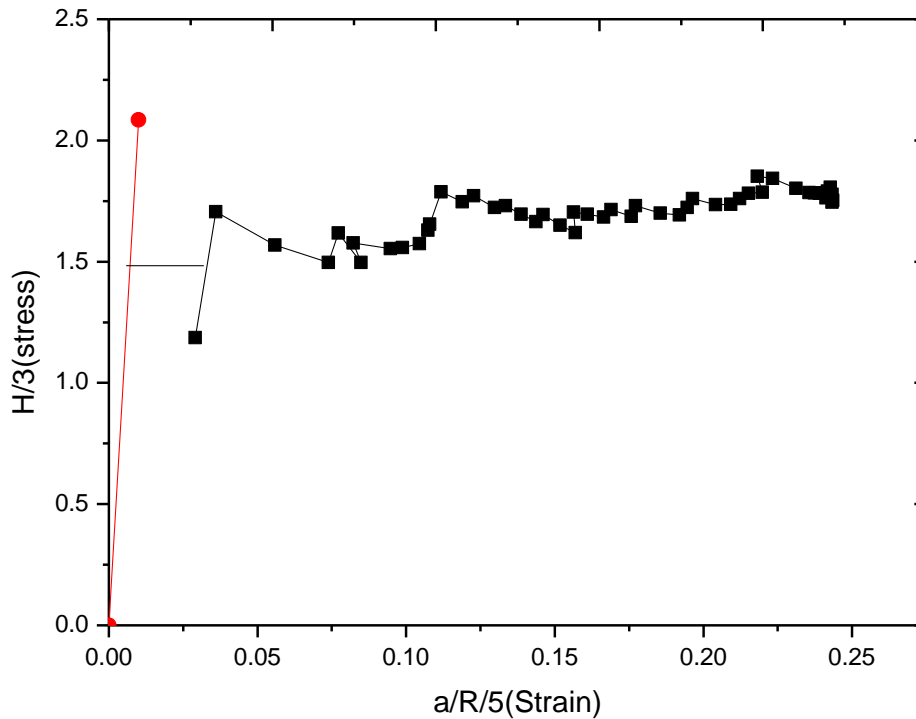


Fig 7.4 the stress-strain curve from nanoindentation before the deformation

The relationship between the stress and strain that a particular material displays is known as that material's Stress-Strain curve. It is unique for each material and is found by recording the amount of deformation (strain) at distinct intervals of tensile or compressive loading (stress).

## 7.2 The modelling for the steel wires

Through reading the papers [57-60], the modelling is a hot topic. As we all know, eutectoid pearlitic steel is an organic combination of ferrite and cementite. As a natural composite material, it is possible to make a model for the cold-drawn steel wires. In this composite material, ferrite plays a role as matrix.

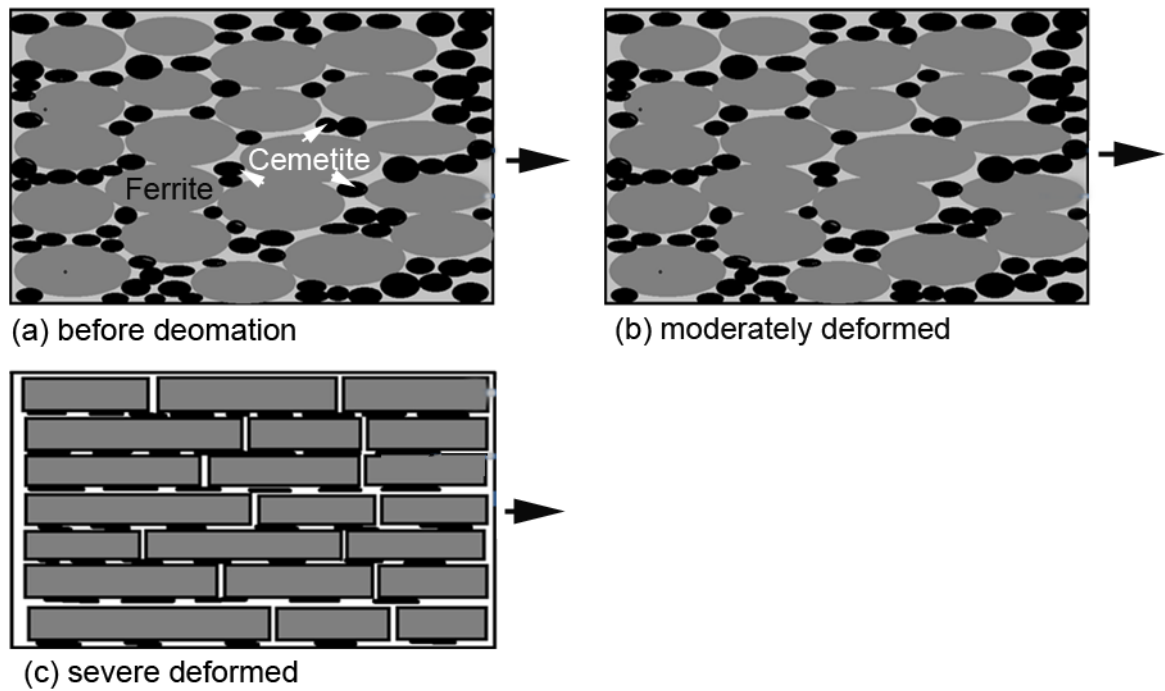


Fig 7.5 Schematic illustration deformation of microstructure morphologies changes of steel wires during drawing process. The arrows indicate the drawing axes.

It is well known that deformation will enhance the changes in microstructure during deformation. The eutectoid pearlitic steel is known as an organic combination of ferrite and cementite. As a natural composite material, it is possible to make a model for the cold-drawn steel wires. In this composite material, ferrite plays a role as matrix. Fig. 7.5 shows the schematic illustration deformation of the microstructure morphologies changes of steel wires during drawing process. There is an angle  $\theta$  between ferrite and cementite. In the microstructure before deformation, ferrite and cementite arrange randomly (Fig. 7.5 (a)). Therefore, it can be assumed the angle  $\theta$  is 45 degree. With the deformation progresses, the angle will be going down. When the drawn wires reach a perfect state, in other words, cementite is parallel to ferrite, the angle should be zero. At the mean time, the steel wires should exhibits the best properties (Fig. 7.5 (c)).

Because of the limited time and equipments, this work has not been done very much. Hopefully, someone will continue this work for designing the better products.

## CHAPTER 8 Summary and Conclusion

### 8.1 summary

In this project, all the research was done on the production and drawing deformation process of high-strength cold-drawing wires. The systematic study has been taken on the microstructure and mechanical properties of high carbon steel wires with drawing strain variation. Through the morphology, microscopic, mechanical and comprehensive analysis, the clear understanding of the organization of high-strength carbon steel wires has been given.

### 8.2 conclusions

Based on the present study, the following general conclusions are made:

After the cold-drawing deformation, the grain the long section of steel wires has been refined significantly. The grain in cross section has been stretched to fibrous, increasing the tensile strength. Before the deformation, the pearlite colony is arranged randomly, the  $\text{Fe}_3\text{C}$  piece is straight and flat. With the increase of deformation, the  $\text{Fe}_3\text{C}$  piece gradually rotates to the drawing axis, basically parallel to the direction.

Pearlite interlamellar spacing decreases with increase of drawing strain. When the strain reach the high level, the change of spacing will be clearer.

The wire strength increases as the rise of drawing deformation, moreover, the increasing speed in high strain is faster than it in the low strain. At the first stage of deformation, the pearlite interlamellar spacing is large, so the hardening accords to the Hall-Petch.

The micro-structural features have been analysed after the cold-drawn deformation. The XRD, FIB and SEM have been used to explore the structure of the steel wires.

The nanoindentation plays a key role in the whole project, measuring the hardness, modulus and stress-strain curve. The model for steel wires has been made for the future products.

### **8.3 Recommendation for Future Work**

1. Because the wire drawing is a complex engineering problem, laboratory cannot be simulated to reproduce the situation of the production site. All samples in this project were collected in the production line. Because the limited space, the samples with different rates of drawing deformation were not collected. But the drawing speed plays a very significant role in the deformation of steel wire. In the future, this work can be done to generate better results.

2. According to papers from Japan and America, the decomposition of cementite is a very hot topic. But, they are all holding the controversial mechanism of cementite decomposition. Because of the limited time as a master student, this work cannot be done very deeply. Hopefully, a clear understanding will be built about this issue.

3. The modelling for steel wires is a good direction to explore the mechanical properties. More work should be done in this field to design the better products to service the society.

---

## CHAPTER 9 References

- [1]. Xiaodan Zhang, Andrew Godfrey, Niels Hansen, et al. *Evolution of cementite morphology in pearlitic steel wire during wet wire drawing*”, Material Scharacterization. 2010, 65 – 72
- [2] Embury JD, Fisher RM. Structure and properties of drawn pearlite. *Acta Metall* 1966;14:147–59.
- [3] Langford G. Study of the deformation of patented steel wire. *Metall Trans* 1970;1:465–77.
- [4] Langford G. Deformation of pearlite. *Metall Trans* 1977;8A:861–75.
- [5] Zelin M. Microstructure evolution in pearlitic steels during wire drawing. *Acta Mater* 2002;50:4431–47.
- [6]. Read HG, Reynolds WT, Hono K, Tarui T. APFIM and TEM studies of drawn pearlitic wire. *Scripta Mater* 1997;37:1221–30.
- [7]. Languillaume J, Kapelski G, Baudalet B. Cementite dissolution in heavily cold drawn pearlitic steel wires. *Acta mater* 1997;45:1201–12.
- [8]. Danoix F, Julien D, Sauvage X, Copreaux J. Direct evidence of cementite dissolution in drawn pearlitic steels observed by tomographic atom probe. *Mater Sci Eng* 1998;250A:8–13.
- [9]. Hono K, Ohnuma M, Murayama M, Nishida S, Yoshie A, Takahashi T. Cementite decomposition in heavily drawn pearlite steel wire. *Scripta Mater* 2001;44:977–83.
- [10]. Gavriljuk V (2002) *Scripta Materialia* 46(2):175
- [11]. J. Toribio, E. Ovejero. *Microstructure orientation in a pearlitic steel subjected to progressive plastic deformation*. *Journal of materials science letters* 17 (1998) 1037-1040
- [12] Xiaodan Zhang, Andrew Godfrey, Niels Hansen, Xiaoxu Huang, Wei Liu, Qing Liu. *Evolution of cementite morphology in pearlite steel wire during wet wire drawing*. *Materials characterization* 61 (2010) 65-72
- [13]. Langford G. Deformation of Pearlite [J]. *Metallurgical Transactions A*, 1977, 8(6): 861-875

- [14]. Langford G. A Study of the Deformation of Patented Steel Wire [J]. Metallurgical Transactions, 1970, 1(2): 465-477
- [15]. Hono K, Ohnuma M, Murayama M, et al. Cementite Decomposition in Heavily Drawn Pearlite Steel Wire [J]. Scripta Materialia, 2001, 44(6): 977-983
- [16]. Toribio J. Relationship between Microstructure and Strength in Eutectoid Steels [J]. Materials Science and Engineering A, 2004, 387-389: 227-230
- [17]. Gavriljuk V G. Decomposition of Cementite in Pearlitic Steel Due to Plastic Deformation [J]. Materials Science and Engineering A, 2003, 345(1-2): 81-89
- [18]. Languillaume J, Kapelski G, Baudelet B. Cementite Dissolution in Heavily Cold Drawn Pearlitic Steel Wires [J]. Acta Materialia, 1997, 45(3): 1201-1212
- [19]. Read H G, Reynolds W T, Hono K, et al. APFIM and Tem Studies of Drawn Pearlitic Wire [J]. Scripta Materialia, 1997, 37(8): 1221-1230
- [20]. Hong M H, Reynolds Jr. W T, Tarui T, et al. Atom Probe and Transmission Electron Microscopy Investigations of Heavily Drawn Pearlitic Steel Wire [J]. Metallurgical and Materials Transactions A: Physical Metallurgy and Materials Science, 1999, 30 A(3): 717-727
- [21]. Sauvage X, Ivanisenko Y. The Role of Carbon Segregation on Nano-crystallization of Pearlitic Steels Processed by Severe Plastic Deformation [J]. Journal of Materials Science, 2007, 42(5): 1615-1621
- [22]. Goto S, Kirchheim R, Al-Kassab T, et al. Application of Cold Drawn Lamellar Microstructure for Developing Ultra-High Strength Wires [J]. Transactions of Nonferrous Metals Society of China, 2007, 17(6): 1129-1138
- [23]. Borchers C, Al-Kassab T, Goto S, et al. Partially Amorphous Nano-composite Obtained From Heavily Deformed Pearlitic Steel [J]. Materials Science and Engineering: A, 2009, 502(1-2): 131-138
- [24]. Gavriljuk V G. Comment on "Effect of Inter-lamellar Spacing on Cementite Dissolution during Wire Drawing of Pearlitic Steel Wires" [J]. Scripta Materialia, 2001, 45(12): 1469-1472

- [25]. Gavriljuk V. Comment On "Cementite Decomposition in Heavily Drawn Pearlite Steel Wire"[J]. *Scripta Materialia*, 2002, 46(2): 175-177
- [26]. Watt P, Van Humbeeck J, Aernoudt E, et al. Strain Ageing in Heavily Drawn Eutectoid Steel Wires[J]. *Scripta Materialia*, 1996, 34(1): 89-95
- [27]. Ohki T, Yaguchi H, Maki K, et al. Change in the Form of Cementite in High Carbon Steel Wires[J]. *Hyperfine Interactions*, 1998, 112(1): 147-150
- [28]. Khrapov A Y, Marks G L, Krechman A F. Concerning Cementite [J]. *Metal Science and Heat Treatment*, 1976, 18(9): 764-766
- [29]. Lee M, Simkovich G. Gibbs Free Energy of Formation of Cementite, Fe<sub>3</sub>C[J]. *Metallurgical and Materials Transactions A*, 1988, 19(8): 2115-2117
- [30]. Sil'Man G I. Effect of Alloying Elements on the Meta-stability of Cementite and its Solubility in Austenite [J]. *Metal Science and Heat Treatment*, 1975, 17(5): 388-391
- [31]. Danoix F, Julien D, Sauvage X, et al. Direct Evidence of Cementite Dissolution in Drawn Pearlitic Steels Observed by Tomographic Atom Probe[J]. *Materials Science and Engineering A*, 1998, 250(1): 8-13
- [32]. Ivanisenko Y, Lojkowski W, Valiev R Z, et al. The Mechanism of Formation of Nanostructure and Dissolution of Cementite in Pearlitic Steel during High Pressure Torsion [J]. *Acta Materialia*, 2003, 51(18): 5555-5570
- [33]. Sauvage X, Guelton N, Blavette D. Microstructure Evolutions During Drawing of a Pearlitic Steel Containing 0.7 at.% Copper[J]. *Scripta Materialia*, 2002, 46(6): 459-464
- [34]. Maruyama N, Tarui T, Tashiro H. Atom Probe Study on the Ductility of Drawn Pearlitic Steels [J]. *Scripta Materialia*, 2002, 46(8): 599-603
- [35]. 樽井敏三 , 丸山直紀. 高炭素線のデラミネーションに及ぼすセメントイト分解の影響[J]. *Tetsu-to-Hagane*, 2004, 90(12): 1031-1037.
- [36]. Seiki Nishida A Y A M. Work Hardening of Hypereutectoid and Eutectoid Steels During Drawing[J]. *ISIJ International* , 1998, 38(2): 177-186

- [37]. Fang X F, Dahl W. Strain Hardening of Steels at Large Strain Deformation. Part I: Relationship between Strain Hardening and Microstructures of B.C.C. Steels [J]. Materials Science and Engineering A, 1995, 203(1-2): 14-25
- [38]. Fang X F, Gusek C O, Dahl W. Strain Hardening of Steels at Large Strain Deformation. Part II: Strain Hardening of Pearlitic and Austenitic Steels and the Estimation of Mechanical Properties[J]. Materials Science and Engineering A, 1995, 203(1-2): 26-35
- [39]. Languillaume J, Kapelski G, Baudalet B. Evolution of the Tensile Strength in Heavily Cold Drawn and Annealed Pearlitic Steel Wires[J]. Materials Letters, 1997, 33(3-4): 241-245
- [40]. Nam W J, Bae C M, Lee C S. Effect of Carbon Content on the Hall-Petch Parameter in Cold Drawn Pearlitic Steel Wires [J]. Journal of Materials Science, 2002, 37(11): 2243-2249
- [41]. Zelin M. Microstructure Evolution in Pearlitic Steels during Wire Drawing [J]. Acta Materialia, 2002, 50(17): 4431-4447
- [42]. Li J, Chou Y. The Role of Dislocations in the Flow Stress Grain Size Relationships [J]. Metallurgical and Materials Transactions B, 1970, 1(5): 1145-1159
- [43]. 横浜国立大学大学院, 光子対の量子状態制御の為の量子ドット技術, <http://www.kmlab.ynu.ac.jp/research.html>, retrieved on Apr 14th, 2011.
- [44]. Laboratory of Inorganic Chemistry, Bragg's Law of Diffraction, <http://www.microscopy.ethz.ch/bragg.htm>, retrieved on Apr 14th, 2011.
- [45]. GuoZhong Cao Nanostructures & nanomaterials: —*Synthesis, properties & applications*//, Imperial College press, USA, 2004.
- [46]. Randall M. German, Seong Jin Park. —*Mathematical relations in particulate materials processing: ceramics, powder metals, hard materials and minerals*//, John Wiley & Sons, Canada, 2008.
- [47]. Sam Zhang, Nasar. Ali. —*Nanocomposite thin films and coatings: processing, properties and performance*//, Imperial College Press: London, 2007.

- [48]. M. ANDRZEJCZUK, T. PŁOCIN' SKI, W. ZIELIN' SKI & K. J . KURZYDŁOWSKI. *TEM characterization of the artefacts induced by FIB in austenitic stainless steel. Journal of Microscopy, Vol. 237, Pt 3 2010, pp. 439–442, 2009*
- [49]. G. M. Hughes<sup>\*1</sup>, G. E. Smith<sup>2</sup>, A. G. Crocker<sup>2</sup> and P. E. J. Flewitt<sup>1,3</sup>. *An experimental and modelling study of brittle cleavage crack propagation in transformable ferritic steel. Materials Science and Technology, 2011 VOL 27.*
- [50]. J.M.Cairney, P.R.Munroe, M.Hoffman. —*The application of focused ion beam technology to the characterizatioin of coatings*//, Surface and Coatings Technology, 2006, 198: 165-168.
- [51]. S.L.Fegler, —*Scanning and transmission dlectron microscopy an introduction*//, W.H. Freeman and company, New York, 1993.
- [52]. X.Cai. H,Bangert. —*Hardness measurement of thin films determining the critical ratio of depth to thickness using FEM*//, Thin Solid Films, 1995, 264: 59-71.
- [53] W.C. Oliver, G.M.Pharr. —*An improved technique for determining hardness and elastic modulus using load and displacement sensing indentation experiments*//, Journal of Materials Research, 1992, 7: 1564-1583.
- [54]. W.C. Oliver, G.M.Pharr. —*An improved technique for determining hardness and elastic modulus using load and displacement sensing indentation experiments*//, Journal of Materials Research, 1992, 7: 1564-1583.
- [55]. W.C. Oliver, G.M.Pharr. —*Measurement of hardness and elastic modulus by instrumented indentation: Advances in understanding and refinements to methodology*//, Journal of Materials Research, 2004, 19: 3-20.
- [56]. Li H. He, Michael V. Swain. —*Nanoindentation derived stress-strain properties of dental materials*//, Dental Materials 23 (2007) 814-821
- [57]. Zonghan Xie, Michael Swain, Paul Munroe, —*on the critical parameters that regulate the deformation behaviour of tooth enamel*//, Biomaterails 29 (2008) 2697-2703
- [58]. Li Hong He, Michael Swain, —*Enamel-A metal-like deformation biocomposite*//, Journal of dentistry 35 (2007) 431-437.

[59]. F. M. Al-Abbasi, —*Micromechanical modelling of ferrite-pearlite steel*//, materials science and Engineering A 527 (2010) 6904-6916.

[60]. Peter Fratzl, Ingo Burgert, Jozef Keckes, —*Mechanical model for the deformation of the wood cell wall*//, Z. Metallked. 95 (2004) 7.

[61]. Maruyama N, Tarui T, Tashiro H. —*Atom Probe Study on the Ductility of Drawn Pearlitic Steels*. Scripta Materials, 2002, 46(8): 599-603.